haematologica
Journal of The Ferrata Storti Foundation

Susceptibility of pediatric acute lymphoblastic leukemia to STAT3 inhibition depends on p53 induction

by Luca Gasparoli, Clemence Virely, Alexia Tsakaneli, Noelia Che, Darren Edwards, Jack Bartram, Michael Hubank, Deepali Pal, Olaf Heidenreich, Joost H.A. Martens, Jasper de Boer, and Owen Williams

Received: May 25, 2023.
Accepted: September 27, 2023.

Citation: Luca Gasparoli, Clemence Virely, Alexia Tsakaneli, Noelia Che, Darren Edwards, Jack Bartram, Michael Hubank, Deepali Pal, Olaf Heidenreich, Joost H.A. Martens, Jasper de Boer, and Owen Williams. Susceptibility of pediatric acute lymphoblastic leukemia to STAT3 inhibition depends on p53 induction. Haematologica. 2023 Oct 5. doi: 10.3324/haematol.2023.283613 [Epub ahead of print]

Susceptibility of pediatric acute lymphoblastic leukemia to STAT3 inhibition depends on p53 induction

Luca Gasparoli[1], Clemence Virely[1], Alexia Tsakaneli[1], Noelia Che[1], Darren Edwards[2], Jack Bartram[2], Michael Hubank[3], Deepali Pal[4], Olaf Heidenreich[5], Joost H.A. Martens[6], Jasper de Boer[1], Owen Williams[1]

[1]Cancer Section, Developmental Biology and Cancer Department, UCL Great Ormond Street Institute of Child Health, London, United Kingdom.

[2]Department of Paediatric Haematology, Great Ormond Street Hospital for Children, London, UK.

[3]Centre for Molecular Pathology, The Royal Marsden, Sutton, UK.

[4]Department of Applied Sciences, Northumbria University, Newcastle upon Tyne, UK. [5]Princess Maxima Centrum for Pediatric Oncology, Utrecht, The Netherlands. [6]Department of Molecular Biology, Faculty of Science, Radboud Institute for Molecular Life Sciences, Radboud University, Nijmegen, The Netherlands.

Short title: The STAT3/p53 axis in pediatric B-ALL

Corresponding author: Owen Williams, Cancer Section, Developmental Biology and Cancer Programme, UCL GOS Institute of Child Health, 30 Guilford Street, London WC1N 1EH, United Kingdom; e-mail: owen.williams@ucl.ac.uk

Data-sharing statement

The authors will make their original data available to future researchers upon request directed to the corresponding author.

Word count: Abstract = 197, Main text = 3,815, 7 Figures, 9 Supplementary figures, 1 Supplementary Table, Supplementary Methods, Supplementary Figure Legends.

Acknowledgements

The authors thank Ayad Eddaoudi, UCL GOS ICH Flow Cytometry Facility, for providing assistance with flow cytometry, all the staff of the UCL GOS ICH Western Laboratories for excellent animal husbandry, and Tony Brooks and Paola Niola, UCL Genomics, for RNA and ChIP sequencing, and Deborah Hughes, Gregorz Pietka, Reda Stankunaite and Paula Proszek at Royal Marsden Hospital Centre for Molecular Pathology for help with TP53 sequencing.

Contributions

LG, CV, AT, NC and OW performed the experiments and data analysis. JB and DE provided clinical input and patient material. MH performed panel sequencing. JHAM analysed ChIP-sequencing data. DP and OH provided primary human MSC samples and methodology for ex vivo PDX co-culture. OW and JdB provided project leadership and supervised the research. LG and OW wrote the paper. All authors read, provided critical comments and approved the manuscript.

Funding

This research was supported by Children with Cancer UK (14-169, 17-249 to Luca Gasparoli); Action Medical Research (GN2368 to Clemence Virely); the Medical Research Council (MR/S021000/1 to Clemence Virely); Children's Cancer and Leukaemia Group Little Princess Trust Project Grant programme (CCLGA 2022 21 to Clemence Virely); SPARKS and Great Ormond Street Hospital Children's Charity

(V4819 to Alexia Tsakaneli); Action Medical Research and Life Arc (GN2820 to Noelia Che); Alternative Hair Charitable Foundation and Great Ormond Street Hospital Children's Charity (W1073 to Jasper de Boer); Great Ormond Street Hospital Children's Charity (V1305, V2617 to Owen Williams); Olivia Hodson Cancer Fund (SR16A35 to Owen Williams); the NIHR Great Ormond Street Hospital Biomedical Research Centre; and an NC3Rs fellowship (NC/P002412/1 to Deepali Pal).

Disclosures: no conflicts of interest to disclose

Abstract

Advances in the clinical management of pediatric B cell Acute Lymphoblastic Leukemia (B-ALL) have dramatically improved outcomes for this disease. However, relapsed and high-risk disease still contribute to significant numbers of treatment failures. Development of new, broad range therapies is urgently needed for these cases. We previously reported the susceptibility of *ETV6-RUNX1*$^{+}$ pediatric B-ALL to inhibition of signal transducer and activator of transcription 3 (STAT3) activity. In the present study, we demonstrate that pharmacological or genetic inhibition of STAT3 results in p53 induction and that CRISPR-mediated *TP53* knockout substantially reverses susceptibility to STAT3 inhibition. Furthermore, we demonstrate that sensitivity to STAT3 inhibition in patient-derived xenograft (PDX) B-ALL samples is not restricted to any particular disease subtype, but rather depends on *TP53* status, the only resistant samples being *TP53* mutant. Induction of p53 following STAT3 inhibition is not directly dependent on MDM2 but correlates with degradation of MDM4. As such, STAT3 inhibition exhibits synergistic *in vitro* and *in vivo* anti-leukemia activity when combined with MDM2 inhibition. Taken together with the relatively low frequency of *TP53* mutations in this disease, these data support the future development of combined STAT3/MDM2 inhibition in the therapy of refractory and relapsed pediatric B-ALL.

Introduction

Pediatric leukemia accounts for up a fifth of all cancer deaths in children. Acute Lymphoblastic Leukemia (ALL) comprises half of these cases, despite the success of modern chemotherapy and risk stratification. Failure of therapy in pediatric ALL is due to refractory and relapsed disease, as well as the toxicity of the chemotherapy itself.[1] There is therefore an unmet clinical need that may be addressed by focussing on inhibition of oncogenic pathways required for leukemia maintenance across a broad range of disease subtypes. Targeting susceptibilities retained in relapsed leukemia is particularly relevant in this context.

Cancer cells often exhibit an exaggerated dependence upon normal cellular signalling pathways. Identification of such pathways deregulated in B-cell precursor ALL (B-ALL) and essential for leukaemia survival is crucial for the development of novel therapies. For example, aberrant activation of STAT3 has been linked with transformation and tumour growth in multiple tissues.[2] Indeed, the importance of STAT3 in hematopoietic malignancies is well documented, particularly for subtypes of lymphoma[3] and acute myeloid leukaemia.[4] Although STAT3 is required for the normal reconstitution activity of hematopoietic stem cells[5,6] its pharmacological targeting does not appear to elicit short-term toxicity,[7] providing a rationale for development of STAT3-targeting drugs.[8] STAT3 is also required for normal B cell development, deficiency resulting in reduced numbers of early B cell progenitors.[9] STAT3-deficient pro-B cells exhibit elevated levels of apoptosis, suggesting that impaired B cell development is caused by loss of B cell progenitor viability in the absence of STAT3.[9]

We previously demonstrated that STAT3 signalling plays an essential role in the most common form of pediatric leukemia, t(12;21) B-ALL. Thus, B-ALL cell lines

containing the t(12;21) chromosomal translocation, which encodes the ETV6-RUNX1 fusion protein, are highly dependent on STAT3 signalling for leukaemia growth, survival, clonogenicity and progression *in vivo.*[10] Furthermore, patient primary *ETV6-RUNX1*$^{+}$ B-ALL cells were also found to be sensitive to STAT3 inhibition. Activation of STAT3 was mediated by an intracellular mechanism downstream of the ETV6-RUNX1 fusion protein, involving guanine nucleotide exchange factor induction.[11] Other B-ALL subtypes, with a much poorer prognosis, were also found to be dependent upon sustained STAT3 activity.[10] More recently, STAT3 dependence has also been demonstrated in poor-risk paediatric B-ALL subtypes, with high STAT3 expression being associated with inferior survival.[12] Although it is likely that there are distinct mechanisms responsible for STAT3 activation in the different B-ALL subtypes, dependency renders them susceptible to pharmacological inhibition of STAT3.

In this study, we used global gene expression analysis to demonstrate that STAT3 inhibition leads to induction of the p53 response in B-ALL cells. Pharmacological inhibition, shRNA-mediated knockdown and CRISPR/Cas9-mediated ablation of *STAT3* all result in elevated p53 protein and p53-target gene expression. B-ALL apoptosis in response to STAT3 inhibition can be reversed by deletion of *TP53*. In contrast to the subtype-specific STAT3 dependence we observed previously in B-ALL cell lines,[10] patient derived xenograft (PDX) B-ALL samples exhibited broad susceptibility to STAT3 inhibition across different subtypes, with resistance only apparent in two *TP53* mutant samples. These data suggest that requirement for STAT3 activity may be a general characteristic of the pediatric B-ALL lineage, perhaps associated with signalling pathways operating in the cells of origin. Enhanced elimination of B-ALL cells was achieved by combining STAT3 inhibition

with p53 induction through inhibition of MDM2, indicating a novel potential therapeutic opportunity. Indeed, since only a minority of paediatric B-ALL cases are associated with *TP53* mutations,[13] even in high-risk and relapsed disease,[14-16] induction of p53 may be an attractive therapeutic approach to leukemias that are refractive to conventional therapy.

Methods

Mice

Mice were maintained in UCL GOSICH animal facilities and experiments were performed according to and approved by United Kingdom Home Office regulations and followed UCL GOSICH institutional guidelines.

B-ALL PDX ALL cells

Ethical approval was given (Research Ethics Committee reference 14/EM/0134) for use of appropriately consented material from patients with B-ALL at Great Ormond Street Hospital for Children (London, UK). 1-2 x 10^6 mononuclear cells (Supplementary Table 1) were intra-bone injected into non-irradiated 6- to 12-week-old NOD-SCID-$\gamma^{-/-}$ (NSG; The Jackson Laboratory, Bar Harbor, ME, USA) mice. Recipient mice were sacrificed upon developing clinical signs of disease. Human PDX ALL cells were harvested and purified from spleens using the mouse cell depletion kit (Miltenyi Biotec, Surrey, UK).

Cell Culture and reagents

For co-culture experiments with Luciferase-expressing B-ALL PDX samples, 3 x $10^4/cm^2$ MSC were plated in 96-well tissue culture plates and 2 x 10^4 B-ALL PDX cells were added in StemSpan Serum-Free Expansion Medium II (SFEM II, STEMCELL Technologies, Cambridge, UK).[17,18] Cells were treated for 5 days with indicated drugs and luminescence analysed with the Steady-Glo Luciferase Assay System (Promega, Southampton, UK), according to manufacturer's instruction, and detected with Infinite m200 Pro microplate reader (Tecan, Reading, UK). The following reagents and inhibitors were used, S3I-201 (Cayman Chemical, MI, United

States), Napabucasin (BBI608; MedChemExpress, NJ, United States), C188-9 (MedChemExpress and Adooq Biosciences, CA, United States), Nutlin-3a (Merck Life Science, Dorset, UK) and Idasanutlin (Bio-Techne, Abingdon, UK).

In vivo transplantation

2 x 10^5 luciferase-expressing B-ALL PDX cells were transplanted intravenously into non-irradiated NSG mice. Recipient mice were imaged using the IVIS® Lumina Series III (PerkinElmer, Beaconsfield, UK) and randomly allocated to control or drug-treated groups, by flipping a coin. Recipient mice were treated with vehicle (7% DMSO, 56% Labrasol, 37% PEG 400), C188-9 (100 mg/kg), Idasanutlin (30 mg/kg) or C188-9 + Idasanutlin by 5-7 daily oral gavages. No blinding was used.

Quantitative RT-PCR (qRT-PCR) analysis

qRT-PCR was performed on mRNA using TaqMan probe-based chemistry, as previously described,[19] using a StepOnePlus Real-Time PCR System (Thermo Fisher Scientific). Primer/probe sets were from Applied Biosystems, Life Technologies.

Western blot and immunoprecipitation (IP) analysis

Western blot and IP analyses were performed as previously described[10,20] (detailed in Supplementary Methods).

RNA sequencing (RNA-seq) and Chromatin immunoprecipitation sequencing (ChIP-seq)

RNA-seq, ChIP-seq, ChIP-qPCR and GSEA was performed as detailed in Supplementary Methods.

Statistics

Statistical significance was determined using Prism (GraphPad) software. Statistical analysis of means was performed using the one sample *t* test or unpaired Student's *t* test, two-tailed *P* values < 0.05 being considered statistically significant. Variance was similar between groups. Statistical analysis of survival curves was performed using the log-rank test.

Data availability

The data generated in this study are available within the article and its Supplementary data files. The RNA-seq data generated in this study are publicly available in the Gene Expression Omnibus at GSE179333 (S3I-201) and GSE179332 (shSTAT3) and the ChIP-seq data at GSE213766. More details are provided in Supplementary Methods.

Results

In order to further investigate the mechanism responsible for STAT3 dependency in *ETV6-RUNX1*$^{+}$ B-ALL, we performed RNA-sequencing (RNA-seq) in REH cells to examine global gene expression changes six hours after pharmacological inhibition of STAT3, via the STAT3 inhibitor S3I-201[21] (Figure 1A). Inhibition of STAT3 resulted in a total of 1085 significantly upregulated and 820 downregulated genes, of which 156 and 22 were changed more than 2-fold, respectively. We performed Gene Set Enrichment analysis (GSEA) with the MSigDB hallmark gene set collection to identify cellular pathways perturbed in this RNA-seq data in an unbiased manner. The hallmark p53 pathway (M5939) gene set was the most upregulated gene set in this analysis (Supplementary Figure S1A). Enrichment of high-confidence p53 target genes, assembled in a recent meta-analysis,[22] confirmed that gene expression changes resulting from acute STAT3 inhibition are consistent with p53 induction (Figure 1B). Analysis of *TP53* RNA sequences from the RNA-seq data confirmed that the REH cells were *TP53* wild-type. Next, we performed RNA-seq in REH cells after shRNA-mediated *STAT3* silencing (Figure 1A, Supplementary Figure S1B). The hallmark p53 pathway was once more the most upregulated gene set (Supplementary Figure S1A) and high-confidence p53 target genes were significantly enriched in these gene expression changes (Figure 1B). Furthermore, 240 of the 1085 genes induced by S3I-201 were also significantly upregulated following *STAT3* silencing, 45 of which were high-confidence p53 target genes.[22] Taken together, these data suggest that STAT3 functions in these cells to repress p53 induction. Direct repression of *TP53* by STAT3 has so far only been demonstrated in transformed fibroblast cells, where STAT3 binds to the promoter of *TP53* and inhibits its transcription.[23] However, we did not observe a significant

change in *TP53* expression in either of the RNA-seq data sets (FC = 1.01, *Padj* = 0.96 and FC = 0.99, *Padj* = 0.83 for *TP53* in the S3I-201 and shSTAT3 data sets, respectively). This indicates that p53 induction resulting from STAT3 inhibition was not due to transcriptional activation of *TP53*.

To examine whether p53 induction following inhibition of STAT3 occurred at the protein level, we examined p53 protein expression after pharmacological or genetic inhibition of STAT3 (Figure 1C-E). Total p53 protein levels increased significantly in REH cells after 6 hours exposure to S3I-201 and an independent STAT3 inhibitor, Napabucasin (BBI608) (Figure 1C).[24] Moreover, this resulted in increased expression of *CDKN1A* (Figure 1F) and other selected p53 target genes (Supplementary Figure S1C). shRNA-mediated silencing of *STAT3* (Supplementary Figure S1B) also resulted in increased total p53 protein and target gene expression (Figure 1D,G). In order to confirm these data using an independent approach, we then targeted *STAT3* in REH cells by CRISPR/Cas9 knockout using two independent gRNAs against the regions encoding the SH2 (g1_STAT3) and DNA-binding (g2_STAT3) domains. Tracking of Indels by DEcomposition (TIDE) analysis in the bulk population of $STAT3^{-/-}$ REH cells confirmed the specific and efficient editing of the targeted regions in *STAT3* (Supplementary Figure S2A) and consequent reduction of total STAT3 protein expression in REH cells (Figure 1E). Loss of STAT3 expression led to selective depletion of $STAT3^{-/-}$ REH cells (Supplementary Figure S2B,C), in line with the anti-proliferative and apoptotic consequences of STAT3 inhibition we described previously.[10] Knockout of STAT3 also resulted in a significant increase in p53 protein (Figure 1E) and target gene (Figure 1H and Supplementary Figure S2D) expression. Conversely, expression of a constitutively active form of

STAT3 (CASTAT3) (Supplementary Figure S3A) we observed a small but significant decrease in p53 target gene expression (Supplementary Figure S3B).

Protein levels of p53 are tightly regulated by the E3 ubiquitin ligase MDM2, which targets p53 for ubiquitination and subsequent degradation.[25-27] To evaluate the role of MDM2 in controlling p53 protein levels in the context of STAT3 inhibition, we performed immunoprecipitation experiments with a specific MDM2 antibody following a short 6-hour exposure to S3I-201. We observed no changes in MDM2 association with p53 (Supplementary Figure S4A), an interaction important for MDM2-regulation of p53 protein expression levels.[28] Furthermore, six hours after exposure, no changes in total MDM2 protein expression were detected following STAT3 inhibition with either S3I-201 or Napabucasin (Supplementary Figure S4B). In contrast, *MDM2* gene expression increased significantly following STAT3 inhibition (Supplementary Figure S4C), most likely as a consequence of p53 induction, since *MDM2* is a well-described p53 target.[29,30] In summary, no changes in MDM2:p53 interaction or total MDM2 protein expression could be detected at a time-point in which p53 induction was evident. Taken together, these data indicate that p53 induction following STAT3 inhibition is not directly dependent on MDM2. Ubiquitination of p53 by MDM2 has also been shown to be positively regulated by MDM4,[31] suggesting an alternative mechanism through which STAT3 could influence p53 protein levels. Although the association of p53 with MDM4 was not affected by 6-hour exposure to S3I-201 (Figure 2A), S3I-201 treatment (Figure 2B) or shRNA-mediated *STAT3* silencing (Figure 2C) resulted in decreased total MDM4 protein expression. Moreover, S3I-201 induced MDM4 loss was rescued by proteasomal inhibition (Figure 2D) suggesting that it was caused by proteasomal degradation. These data indicate that p53

induction correlates with reduced levels of MDM4 protein expression following STAT3 inhibition.

We speculated that the observed increase in p53 protein expression would translate into increased binding to target gene loci. Indeed, immunoprecipitation experiments following STAT3 inhibition by S3I-201 revealed a significant increase in the mono-methylation of lysine 372 of p53 (Figure 3A), a post-translational modification of p53 associated with increased DNA binding, resulting from the increase in total p53.[32] Increased binding of target loci by p53 was confirmed by ChIP-seq (Figure 3B,C and Supplementary Figure S4D) and ChIP-qPCR (Figure 3D) experiments. S3I-201 exposure resulted in more than 2-fold increased binding of p53 at 400 peaks in REH cells (Figure 3B), including well-established p53 target genes *CDKN1A,*[33] *BBC3* (PUMA)[34] and ATF3[35] (Figure 3C-D). GSEA revealed significant enrichment of the genes that were associated with increased p53 binding in gene expression changes following S3I-201 treatment of REH cells (Figure 3E).

To determine the contribution of p53 induction to the response of REH cells to STAT3 inhibition, we performed CRISPR/Cas9-mediated knockout of *TP53* in REH cells. Loss of p53 protein was confirmed in two independent *TP53*$^{-/-}$ clones (Figure 4A). TIDE analysis of the *TP53*$^{-/-}$ clones confirmed specific and efficient editing of the targeted region encoding the N-terminus domain of p53 (Supplementary Figure S5A). As expected, loss of *TP53* abrogated the induction of p53 target gene expression resulting from STAT3 inhibition (Figure 4B) and significantly attenuated apoptosis induction following STAT3 inhibition with either S3I-201 or Napabucasin (Figure 4C). Similar impairment of apoptosis induction was observed following treatment of *TP53*$^{-/-}$ REH clones with the MDM2 inhibitor Nutlin-3a (Figure 4D). Moreover, *TP53* loss also rescued inhibition of REH cell colony formation in

methylcellulose following STAT3 inhibition (Supplementary Figure S5B). In contrast, S3I-201-iduced loss of MDM4 protein was not affected by *TP53* knockout, confirming that although p53 has been shown to repress *MDM4* mRNA translation[31] this was not the cause of MDM4 loss following STAT3 inhibition (Supplementary Figure S5C).

We demonstrated previously that *ETV6-RUNX1*$^{+}$ B-ALL cell lines and primary patient samples are highly dependent on STAT3 signalling for leukemia growth, survival, clonogenicity and progression *in vivo.*[10] In order to investigate STAT3 dependence across different paediatric B-ALL subtypes, we expanded our analysis to B-ALL patient-derived xenograft (PDX) samples, including some generated from relapsed B-ALL cases. 12/14 B-ALL PDX samples exhibited sensitivity to 24-hour S3I-201 exposure (Figure 5A). Interestingly, sensitivity was apparent across a broad range of B-ALL subtypes, including *ETV6-RUNX1*$^{+}$ but also *TCF3-PBX1*$^{+}$, Hyperdiploid, *KMT2A*-rearranged and *PAX5* rearranged samples, and samples from relapsed disease. In contrast, an *ETV6-RUNX1*$^{+}$ and a Hypodiploid B-ALL PDX sample, both from relapsed disease, exhibited resistance to STAT3 inhibition (Figure 5A). Upregulation of *CDKN1A* and *GADD45A* gene expression after 6-hour S3I-201 treatment followed the same pattern of response, changes in expression being detected in sensitive but not resistant samples (Figure 5B). Total p53 protein levels increased in all B-ALL PDX samples 6 hours after exposure to S3I-201 (Supplementary Figure S6A-C). The pattern in loss of viability was the same upon exposure of the PDX samples to Nutlin-3a, with the two S3I-201-resistant samples also exhibiting resistance to MDM2 inhibition (p53 induction) (Figure 5C). Sanger sequencing of the diagnostic relapse hypodiploid B-ALL sample from which one of the resistant PDX (sample 14) was generated, revealed the presence of a missense heterozygous *TP53* mutation (Supplementary Figure S7A). Targeted gene panel

sequencing of the other resistant B-ALL PDX (sample 13), derived from relapsed *ETV6-RUNX1*$^{+}$ disease, detected three mutations affecting *TP53* (Supplementary Figure S7B). *TP53* missense mutations in both samples affected the region encoding the DNA binding domain of p53, Y220C and R248Q in the hypodiploid and *ETV6-RUNX1*$^{+}$ samples, respectively. In contrast, targeted gene panel sequencing of the 12 sensitive PDX samples confirmed their wild-type *TP53* status, although one of these (sample 11) contained a heterozygous deletion (chr17p11.2-p13.3) encompassing one *TP53* allele. Taken together, these data are consistent with a critical role of p53 in mediating B-ALL sensitivity to STAT3 inhibition.

Since p53 induction following STAT3 inhibition did not appear to be mediated via direct MDM2 modulation (Supplementary Figure S4A-C), we reasoned that it may synergise with p53 induction resulting from MDM2 inhibition. Indeed, inhibition of STAT3 by either S3I-201 or Napabucasin demonstrated synergistic anti-leukemia activity in REH cells, when combined with MDM2 inhibition by Nutlin-3a (Figure 6A,B), suggesting a rationale for combined targeting of STAT3 and MDM2 in novel B-ALL therapy.

We next used a previously developed co-culture model in which drug susceptibility of luciferase-expressing B-ALL PDX samples is evaluated after seeding onto primary Nestin-positive human mesenchymal stem cells (MSC).[18] Five luciferase-transduced B-ALL PDX samples, two of which came from relapsed disease, proliferated over a 5-day period on human MSC (Supplementary Figure S8A). All of these samples exhibited sensitivity to C188-9[36] (also known as TTI-101), a more potent STAT3 inhibitor than S3I-201, over a similar concentration range to those reported for solid cancer cells[37] (Supplementary Figure S8B). Increased susceptibility of all five samples to STAT3 inhibition (by S3I-201, Napabucasin or

C188-9) was evident on combination with MDM2 inhibition (Figure 6C). The anti-leukemia effect observed in this co-culture model was associated with cell death (Supplementary Figure S8C) and was not a consequence of a direct effect of the drugs on primary MSC viability (data not shown). In contrast, these drug combinations had virtually no effect on the luciferase-expressing *TP53* mutant hypodiploid B-ALL PDX (sample 14) (Supplementary Figure S8D). Similar responses to drug combinations occurred in three additional untransduced PDX samples (Supplementary Figure S8E). Longitudinal bioluminescence imaging demonstrated that short-term oral administration of Idasanutlin (MDM2 inhibitor) impaired disease progression *in vivo* in the *PAX5* rearranged (sample 11) relapsed (Figure 7) and the *KMT2A-MLLT3*$^{+}$ (sample 9) B-ALL model (Supplementary Figure S9A,B), and that in the former efficacy was improved by combining MDM2 with STAT3 inhibition.

Discussion

In this study we demonstrate that pediatric pre-B ALL exhibits broad sensitivity to STAT3 inhibition. Previously, we demonstrated that *ETV6-RUNX1*$^{+}$ B-ALL cell lines and primary patient samples were susceptible to inhibition of STAT3.[10,11] However, in contrast to cell lines,[10] the present study demonstrates that susceptibility of PDX samples is not restricted to specific subtypes of B-ALL but appears to be a general feature of the disease. Pharmacologic, shRNA- or CRISPR/Cas9-mediated inhibition of STAT3 resulted in p53 induction and cell death, largely abrogated by CRISPR-Cas9 mediated *TP53* knockout. Furthermore, two PDX samples exhibiting resistance to STAT3 inhibition were also resistant to MDM2 inhibition and contained missense *TP53* mutations. Taken together, these data indicate that p53 induction underlies the sensitivity of B-ALL cells to STAT3 inhibition.

Combined C188-9 and Idasanutlin treatment was more effective at impairing disease progression in comparison to Idasanutlin alone in the *PAX5* rearranged B-ALL PDX sample. These data validate the enhanced sensitivity of B-ALL PDX samples to combined STAT3 and MDM2 inhibition *in vitro*. However, enhanced drug combination efficacy was not seen *in vivo* for the *KMT2A-MLLT3*$^{+}$ sample and C188-9 alone did not affect disease progression in either sample. The difference in effectiveness of Idasanutlin and C188-9 *in vivo* is likely to be due to their relative bioavailabilities, further improvements of which will be required for translation of STAT3 inhibition as a therapy in B-ALL.

Evidence in the literature indicates that p53 may be regulated by STAT3 through a variety of different mechanisms. Transcriptional repression of *TP53* by STAT3 was demonstrated in Src transformed fibroblasts and melanoma cells,[23] and in chronic lymphocytic leukemia B cells.[38] More recently, leukemia inhibitory factor (LIF) was

also shown to cause STAT3-dependent reduction in p53 protein expression levels in colorectal cancer cells.[39] However, in this case STAT3 activation had no effect on *TP53* mRNA levels but was rather shown to act via indirect transcriptional activation of *MDM2* and consequent p53 protein degradation.[39] Similarly, we did not observe any change in *TP53* expression in B ALL cells following STAT3 inhibition, but p53 regulation was not directly dependent on MDM2 either. However, STAT3 inhibition resulted in MDM4 protein loss that was rescued by proteasomal inhibition and was not a result of p53 induction. Since MDM4 has been shown to increase ubiquitination of p53 by MDM2, as well as directly inhibiting the transactivation activity of p53,[31] it is likely that STAT3 inhibition leads to elevated p53 protein levels by inducing MDM4 degradation. Further experiments are necessary to elucidate exactly how this is achieved.

The broad susceptibility of pediatric B-ALL PDX samples to STAT3 inhibition suggests that a requirement for STAT3 activity may be a general characteristic of the pediatric B-ALL lineage, perhaps associated with signalling pathways operating in the cells of origin. In this context it is worth noting that both STAT3 and p53 play important roles in normal B cell development. Thus, STAT3 was shown to be involved in the positive regulation of B cell development, deficiency resulting in a partial pre-pro-B cell differentiation block and increased pro-B cell apoptosis.[9] With respect to p53, regulation of its expression, transcriptionally or otherwise, plays a critical role in pre-B cells development and selection. For example, apoptosis of pre-B cells that fail to productively rearrange their immunoglobulin heavy chain genes was shown to be mediated by p53 induction.[40] In this case, induction was via transcriptional activation of *TP53* by the transcription factor BACH2. Furthermore, BACH2 was shown to act as a tumour suppressor in pre-B ALL, by virtue of its

regulation of *TP53* expression.[40] Signalling pathways regulating p53 activity also appear to control pre-B cell homeostasis. The Wip1 phosphatase, encoded by the p53 target gene *PPM1D*, is involved in the negative feedback regulation of p53 activation.[41] Interestingly, deletion of the *Ppm1d* gene was shown to result in reduced numbers of mature B cells. This defect was found to be due to induction of p53 and apoptosis in the pre-B cell compartment and could be reversed by deletion of *Tp53.*[42] This suggests that the autoregulatory loop between Wip1 and p53 functions to maintain normal pre-B cell development.

In contrast to the evidence for isolated STAT3 and p53 function in normal B cell development, relatively little is known about the possible connection between STAT3 activity and repression of p53 induction in B cell progenitors. In this context, it is interesting to note that constitutively active STAT3 was shown to promote resistance to gamma irradiation-induced apoptosis in peritoneal B-1 cells.[43] Interestingly, STAT3-dependent radioresistance could also be induced in normal B-2 B cells by stimulation with cytokines in the presence of BCR cross-linking.[43] Although p53 induction by gamma irradiation was not directly examined in this study, these data suggest that a link may exist between STAT3 activity and suppression of p53 responses in normal B cells. Further studies will be required to establish whether the STAT3/p53 pathway we describe in pre-B ALL is associated with leukemogenesis or rather is retained during transformation of pre-B cells.

TP53 mutations are more prevalent in relapsed pediatric B-ALL than primary disease.[14-16] Indeed, thiopurine chemotherapy has recently been linked with the emergence of missense *TP53* mutations.[44] However, the overall incidence of these mutations is still relatively low in comparison to other cancers,[13,45] supporting the

therapeutic applicability of this approach to p53 induction in primary and relapsed pediatric B-ALL.

In conclusion, we demonstrate broad susceptibility of pediatric B ALL to p53 induction following STAT3 and combined STAT3/MDM2 inhibition. p53 induction is not a result of increased *TP53* transcription and is not directly dependent on MDM2, but rather is likely to result from MDM4 degradation. Consistent with this, B-ALL cells exhibited increased sensitivity to combined STAT3 and MDM2 inhibition *in vitro* and *in vivo*, indicating a novel disease susceptibility amenable to therapeutic exploitation.

References

1. Karol SE, Pui CH. Personalized therapy in pediatric high-risk B-cell acute lymphoblastic leukemia. Ther Adv Hematol. 2020;11:2040620720927575.
2. Yu H, Lee H, Herrmann A, Buettner R, Jove R. Revisiting STAT3 signalling in cancer: new and unexpected biological functions. Nat Rev Cancer. 2014;14(11):736-746.
3. Zhu F, Wang KB, Rui L. STAT3 Activation and Oncogenesis in Lymphoma. Cancers (Basel). 2019;12(1):19.
4. Bar-Natan M, Nelson EA, Xiang M, Frank DA. STAT signaling in the pathogenesis and treatment of myeloid malignancies. JAKSTAT. 2012;1(2):55-64.
5. Oh IH, Eaves CJ. Overexpression of a dominant negative form of STAT3 selectively impairs hematopoietic stem cell activity. Oncogene. 2002;21(31):4778-4787.
6. Chung YJ, Park BB, Kang YJ, Kim TM, Eaves CJ, Oh IH. Unique effects of Stat3 on the early phase of hematopoietic stem cell regeneration. Blood. 2006;108(4):1208-1215.
7. Kortylewski M, Kujawski M, Wang T, et al. Inhibiting Stat3 signaling in the hematopoietic system elicits multicomponent antitumor immunity. Nat Med. 2005;11(12):1314-1321.
8. Frank DA. STAT3 as a central mediator of neoplastic cellular transformation. Cancer Lett. 2007;251(2):199-210.
9. Chou WC, Levy DE, Lee CK. STAT3 positively regulates an early step in B-cell development. Blood. 2006;108(9):3005-3011.

10. Mangolini M, de Boer J, Walf-Vorderwulbecke V, Pieters R, den Boer ML, Williams O. STAT3 mediates oncogenic addiction to TEL-AML1 in t(12;21) acute lymphoblastic leukemia. Blood. 2013;122(4):542-549.
11. Virely C, Gasparoli L, Mangolini M, et al. ARHGEF4 Regulates an Essential Oncogenic Program in t(12;21)-Associated Acute Lymphoblastic Leukemia. Hemasphere. 2020;4(5):e467.
12. Bhansali RS, Rammohan M, Lee P, et al. DYRK1A regulates B cell acute lymphoblastic leukemia through phosphorylation of FOXO1 and STAT3. J Clin Invest. 2021;131(1):e135937.
13. Imamura J, Miyoshi I, Koeffler HP. p53 in hematologic malignancies. Blood. 1994;84(8):2412-2421.
14. Gump J, McGavran L, Wei Q, Hunger SP. Analysis of TP53 mutations in relapsed childhood acute lymphoblastic leukemia. J Pediatr Hematol Oncol. 2001;23(7):416-419.
15. Hof J, Krentz S, van Schewick C, et al. Mutations and deletions of the TP53 gene predict nonresponse to treatment and poor outcome in first relapse of childhood acute lymphoblastic leukemia. J Clin Oncol. 2011;29(23):3185-3193.
16. Krentz S, Hof J, Mendioroz A, et al. Prognostic value of genetic alterations in children with first bone marrow relapse of childhood B-cell precursor acute lymphoblastic leukemia. Leukemia. 2013;27(2):295-304.
17. Bomken S, Buechler L, Rehe K, et al. Lentiviral marking of patient-derived acute lymphoblastic leukaemic cells allows in vivo tracking of disease progression. Leukemia. 2013;27(3):718-721.

18. Pal D, Blair HJ, Elder A, et al. Long-term in vitro maintenance of clonal abundance and leukaemia-initiating potential in acute lymphoblastic leukaemia. Leukemia. 2016;30(8):1691-1700.

19. Walf-Vorderwulbecke V, Pearce K, Brooks T, et al. Targeting acute myeloid leukemia by drug-induced c-MYB degradation. Leukemia. 2018;32(4):882-889.

20. Clesham K, Walf-Vorderwulbecke V, Gasparoli L, et al. Identification of a c-MYB-directed therapeutic for acute myeloid leukemia. Leukemia. 2022;36(6):1541-1549.

21. Siddiquee K, Zhang S, Guida WC, et al. Selective chemical probe inhibitor of Stat3, identified through structure-based virtual screening, induces antitumor activity. Proc Natl Acad Sci U S A. 2007;104(18):7391-7396.

22. Fischer M. Census and evaluation of p53 target genes. Oncogene. 2017;36(28):3943-3956.

23. Niu G, Wright KL, Ma Y, et al. Role of Stat3 in regulating p53 expression and function. Mol Cell Biol. 2005;25(17):7432-7440.

24. Li Y, Rogoff HA, Keates S, et al. Suppression of cancer relapse and metastasis by inhibiting cancer stemness. Proc Natl Acad Sci U S A. 2015;112(6):1839-1844.

25. Haupt Y, Maya R, Kazaz A, Oren M. Mdm2 promotes the rapid degradation of p53. Nature. 1997;387(6630):296-299.

26. Kubbutat MH, Jones SN, Vousden KH. Regulation of p53 stability by Mdm2. Nature. 1997;387(6630):299-303.

27. Honda R, Tanaka H, Yasuda H. Oncoprotein MDM2 is a ubiquitin ligase E3 for tumor suppressor p53. FEBS Lett. 1997;420(1):25-27.

28. Lane DP, Hall PA. MDM2--arbiter of p53's destruction. Trends Biochem Sci. 1997;22(10):372-374.

29. Barak Y, Juven T, Haffner R, Oren M. mdm2 expression is induced by wild type p53 activity. EMBO J. 1993;12(2):461-468.

30. Wu X, Bayle JH, Olson D, Levine AJ. The p53-mdm-2 autoregulatory feedback loop. Genes Dev. 1993;7(7A):1126-1132.

31. Haupt S, Mejia-Hernandez JO, Vijayakumaran R, Keam SP, Haupt Y. The long and the short of it: the MDM4 tail so far. J Mol Cell Biol. 2019;11(3):231-244.

32. Chuikov S, Kurash JK, Wilson JR, et al. Regulation of p53 activity through lysine methylation. Nature. 2004;432(7015):353-360.

33. el-Deiry WS, Tokino T, Velculescu VE, et al. WAF1, a potential mediator of p53 tumor suppression. Cell. 1993;75(4):817-825.

34. Nakano K, Vousden KH. PUMA, a novel proapoptotic gene, is induced by p53. Mol Cell. 2001;7(3):683-694.

35. Zhang C, Gao C, Kawauchi J, Hashimoto Y, Tsuchida N, Kitajima S. Transcriptional activation of the human stress-inducible transcriptional repressor ATF3 gene promoter by p53. Biochem Biophys Res Commun. 2002;297(5):1302-1310.

36. Redell MS, Ruiz MJ, Alonzo TA, Gerbing RB, Tweardy DJ. Stat3 signaling in acute myeloid leukemia: ligand-dependent and -independent activation and induction of apoptosis by a novel small-molecule Stat3 inhibitor. Blood. 2011;117(21):5701-5709.

37. Lewis KM, Bharadwaj U, Eckols TK, et al. Small-molecule targeting of signal transducer and activator of transcription (STAT) 3 to treat non-small cell lung cancer. Lung Cancer. 2015;90(2):182-190.

38. Sainz-Perez A, Gary-Gouy H, Gaudin F, et al. IL-24 induces apoptosis of chronic lymphocytic leukemia B cells engaged into the cell cycle through dephosphorylation of STAT3 and stabilization of p53 expression. J Immunol. 2008;181(9):6051-6060.

39. Yu H, Yue X, Zhao Y, et al. LIF negatively regulates tumour-suppressor p53 through Stat3/ID1/MDM2 in colorectal cancers. Nat Commun. 2014;5:5218.

40. Swaminathan S, Huang C, Geng H, et al. BACH2 mediates negative selection and p53-dependent tumor suppression at the pre-B cell receptor checkpoint. Nat Med. 2013;19(8):1014-1022.

41. Takekawa M, Adachi M, Nakahata A, et al. p53-inducible wip1 phosphatase mediates a negative feedback regulation of p38 MAPK-p53 signaling in response to UV radiation. EMBO J. 2000;19(23):6517-6526.

42. Yi W, Hu X, Chen Z, et al. Phosphatase Wip1 controls antigen-independent B-cell development in a p53-dependent manner. Blood. 2015;126(5):620-628.

43. Otero DC, Poli V, David M, Rickert RC. Cutting edge: inherent and acquired resistance to radiation-induced apoptosis in B cells: a pivotal role for STAT3. J Immunol. 2006;177(10):6593-6597.

44. Yang F, Brady SW, Tang C, et al. Chemotherapy and mismatch repair deficiency cooperate to fuel TP53 mutagenesis and ALL relapse. Nat Cancer. 2021;2(8):819-834.

45. Comeaux EQ, Mullighan CG. TP53 Mutations in Hypodiploid Acute Lymphoblastic Leukemia. Cold Spring Harb Perspect Med. 2017;7(3):a026286.

Figure Legends

Figure 1. STAT3 inhibition results in p53 induction in B-ALL cells. A Volcano plots of RNA-seq analysis showing fold gene expression changes in REH cells following treatment with S3I-201 (50 μM, 6h, n=3) or 5 days after shRNA-mediated *STAT3* (sh1, n=3) silencing. Expression changes greater than 2-fold and $P < 0.05$ are shown in red, Wald test. **B** GSEA demonstrating enrichment of p53 target genes, as previously defined in [22], in S3I-201 and shSTAT3 induced gene expression changes. **C-E** Western blot examples (top panels) and quantification (lower panels) of p53 protein expression in REH cells **C** 6h after exposure to S3I-201 (50 μM) or Napabucasin (10 μM), **D** 5 days after transduction with scrambled control or shSTAT3 (sh1) shRNA or **E** 7 days after transduction with Cas9 and control or gSTAT3 gRNA. Bars and error bars are means and SD of **C** n=8 and **D**, **E** n=4 independent experiments. Data are normalized to **C**, **D** tubulin and **E** GAPDH loading control and to **C** DMSO-treated, **D** control shRNA transduced and **E** control gRNA transduced REH cells. *$P < 0.05$; **$P < 0.01$; ***$P < 0.001$, one sample *t* test. **F-H** qRT-PCR analysis of *CDKN1A* gene expression in REH cells **F** 6h after exposure to S3I-201 (50 μM) or Napabucasin (10 μM), **G** 5 days after transduction with scrambled control or shSTAT3 shRNA or **H** 7 days after transduction with Cas9 and control or gSTAT3 gRNA. Bars and error bars are means and SD of **F** n=5, **G** n=4 and **H** n=5 independent experiments. Gene expression data are normalised to **F** DMSO-treated, **G** control shRNA transduced and **H** control gRNA transduced REH cells. *$P < 0.05$; **$P < 0.01$; ***$P < 0.001$, one sample *t* test.

Figure 2. p53 induction following STAT3 inhibition correlates with loss of MDM4. A Western blot analysis (left panel) and p53 protein expression quantification

(right panel) of input and anti-MDM4 immunoprecipitates from REH cells, following 6 hours treatment with S3I-201 (50 μM). Blots were stained with anti-p53 or anti-MDM4. Data are normalized to DMSO-treated REH cells. Bars and error bars are means and SD of n=3 independent experiments. *$P < 0.05$; n.s. not significant, one sample *t*-test. **B-C** Western blot analysis (left panels) and quantification (right panels) of MDM4 and p53 protein expression in REH cells following **B** 6h treatment with S3I-201 (50 μM) or **C** 5 days after transduction with scrambled control or shSTAT3 (sh1) shRNA. GAPDH was used as a loading control. Bars and error bars are means and SD of n=3 independent experiments. Data are normalized to GAPDH loading control and to DMSO-treated REH cells. *$P < 0.05$; **$P < 0.01$; n.s. not significant, one sample *t*-test. **D** Western blot analysis (left panel) and quantification (right panel) of MDM4 protein expression in REH cells following 6h treatment with S3I-201 (50 μM), with and without MG132 (10μM). GAPDH was used as a loading control. Bars and error bars are means and SD of n=3 independent experiments. Data are normalized to GAPDH loading control and to DMSO-treated REH cells. *$P < 0.05$; n.s. not significant, one sample *t*-test.

Figure 3. STAT3 inhibition results in increased binding of p53 to target genes. **A** Western blot example (left panel) and quantification (right panel) of input and anti-$p53^{K372me1}$ immunoprecipitates from REH cells, following 6h treatment with DMSO or S3I-201 (50 μM), stained with anti-p53 (DO-1). Bar and error bars are means and SD of n=3 independent experiments. Data are normalised to DMSO-treated cells. **$P < 0.01$, one sample *t* test. **B** Heatmap showing ChIP signal for the dynamic p53 peaks (>2-fold increased in S3I-201 with over 100 counts per million reads) following 6 hours exposure to DMSO or S3I-201 (50 μM). **C** Exemplar ChIP-Seq tracks for p53

peaks at target genes in DMSO and S3I-201 treated REH cells. High-confidence (*CDKN1A*, *ATF3*) p53 binding motifs are indicated by vertical black bars below the scale ruler. **D** ChIP-qPCR validation analysis of p53 binding at *CDKN1A* (top panel), *BBC3* (middle panel) and *ATF3* (lower panel) in REH cells following 6h treatment with S3I-201 (50 μM). Data are shown as fold increase of enrichment over that from a gene desert region, normalised to DMSO-treated cells. Bars and error bars are means and SD of n=3 independent experiments. **P* < 0.05; ***P* < 0.01, one sample *t* test. **E** GSEA demonstrating enrichment of 122 genes, with >2-fold increased p53 binding with peaks over 100 cpm reads, in gene expression changes in REH cells following treatment with S3I-201 (Figure 1A).

Figure 4. *TP53* knock-out desensitises B-ALL cells to STAT3 inhibition. A Western blot analysis of p53 protein expression in REH cells and *TP53*^{wt} and *TP53*$^{-/-}$ clones, obtained by transduction of REH cells with Cas9 and control or *TP53*-specific gRNA, clones from the latter being selected for loss of p53 protein expression. **B** qRT-PCR analysis of selected p53 target gene[22] expression in *TP53*^{wt} and *TP53*$^{-/-}$ REH clones following 6h treatment with S3I-201 (50 μM). Gene expression data are normalised to gene expression in the DMSO-treated *TP53*^{wt} clone. Bars and error bars are means and SD of n=4 independent experiments. **P* < 0.05; ***P* < 0.01; ****P* < 0.001, unpaired Student's *t* test between S3I-201-treated *TP53*^{wt} and *TP53*$^{-/-}$ clones. **C** Induction of apoptosis (% Annexin V^{+} cells) in *TP53*^{wt} and *TP53*$^{-/-}$ REH clones following 48 hours treatment with S3I-201 (50 μM) or Napabucasin (10 μM). Bars and error bars are means and SD of n=5 independent experiments. ***P* < 0.01; ****P* < 0.001, unpaired Student's *t* test between S3I-201- or Napabucasin-treated *TP53*^{wt} and *TP53*$^{-/-}$ clones. **D** Induction of apoptosis (%

Annexin V^+ cells) in *TP53*^{wt} and *TP53*$^{-/-}$ REH clones following 48 hours treatment with indicated concentrations of Nutlin-3a. Bars and error bars are means and SD of n=3 independent experiments. $^{**}P < 0.01$; $^{***}P < 0.001$, unpaired Student's *t* test between Nutlin 3a-treated *TP53*^{wt} and *TP53*$^{-/-}$ clones.

Figure 5. The sensitivity of B-ALL PDX cells to STAT3 inhibition correlates with *TP53* status. A Induction of apoptosis (% Annexin V^+ cells) in B-ALL PDX samples following 24h treatment with S3I-201 (50 μM) in liquid culture. B-ALL PDX samples: *ETV6-RUNX1*$^+$ (1-5, 12, 13), *TCF3-PBX1*$^+$ (6), Hyperdiploid (7), High-Hyperdiploid (8), *KMT2A-MLLT3*$^+$ (9), *KMT2A-AFDN*$^+$ (10), *PAX5* rearranged (11) and Hypodiploid (14). Samples 1-10 were derived from presentation samples and samples 11-14 from relapsed samples. **B** qRT-PCR analysis of *CDKN1A* and *GADD45A* gene expression in B-ALL PDX samples following 6h treatment with S3I-201 (50 μM). Gene expression data are normalised to DMSO-treated cells. **C** Induction of apoptosis (% Annexin V^+ cells) in B-ALL PDX samples following 24h treatment with Nutlin-3a (5 μM) in liquid culture.

Figure 6. STAT3 and MDM2 inhibition synergise in triggering cell death in B-ALL cells. A Viability of REH cells following 72h treatment with indicated concentrations of either S3I-201 or Napabucasin in combination with Nutlin-3a. Data are normalised to DMSO-treated cells. Graphs points and error bars are means and SD of n=4 (S3I-201) and n=3 (Napabucasin) independent experiments. **B** 3D synergy maps and ZIP synergy scores of data shown in **A**, calculated with SynergyFinder (version 2.0). **C** Luminescence of luciferase-expressing B-ALL PDX samples, grown in co-culture with human MSC, 5 days after exposure to MDM2

inhibitor Nutlin-3a (5 μM) alone or in combination with STAT3 inhibitors S3I-201 (50 μM), Napabucasin (1.5 μM) and C188-9 (10 μM). Corresponding B-ALL PDX sample number from Figure 4 is indicated in brackets. Data are normalised to DMSO-treated cells. Bars and error bars are means and SD of n=3 independent experiments. *P < 0.05; **P < 0.01; ***P < 0.001; n.s. not significant, one sample t test.

Figure 7. STAT3 and MDM2 inhibition impair B-ALL progression *in vivo*. A Bioluminescence signal (radiance = photons/s/cm2/steradian) in NSG recipient mice 5 days after injection of the luciferase-expressing *PAX5* rearranged (relapse) B-ALL PDX sample and before drug treatment (left panel), and fold change in bioluminescence signal 11 days after injection, following 5 daily treatments with vehicle or the indicated drug combinations (right panel). Bars and error bars are means and SD of values form each treatment group, the number of mice in each group indicated in brackets. *P < 0.05; ***P < 0.001; n.s. not significant, unpaired Student's t test between indicated groups. **B** Bioluminescence imaging of NSG recipient mice before (day 5) and after (day 11) drug treatment. Bars for luminescence signal represent photons/s/cm2/steradian. **c** Survival curve for recipient mice in **A**, **B**, treated with vehicle (black solid line), C188-9 (black dashed line), Idasanutlin (IDA, red dashed line) or C188-9 + IDA combination (red solid line). Red arrows indicate drug treatments. P = 0.76 (vehicle versus C188-9); P = 0.055 (vehicle versus IDA); P = 0.0131 (vehicle versus C188-9 + IDA); P = 0.0494 (IDA versus C188-9 + IDA), log-rank test.

Figure 1

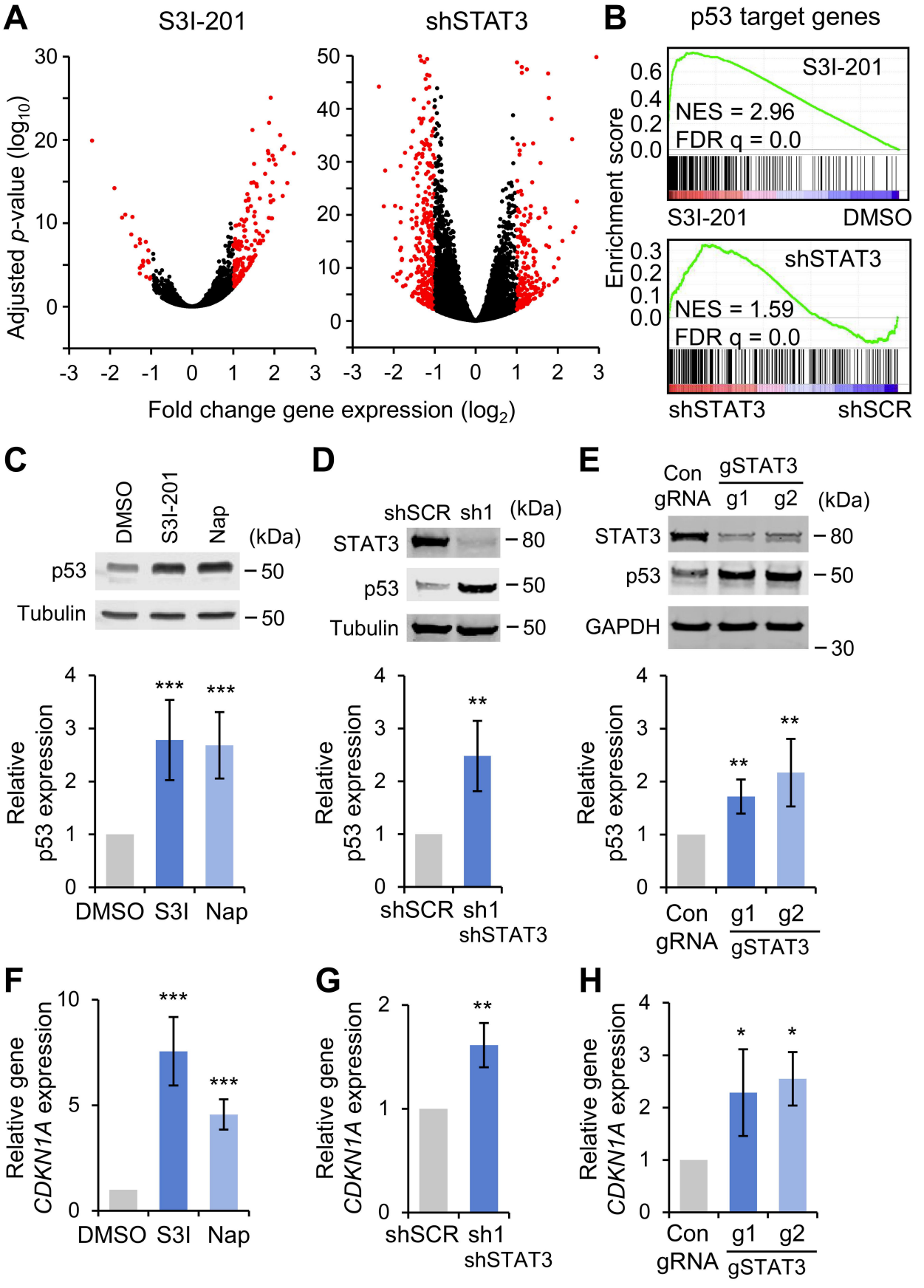
A
S3I-201
shSTAT3
Adjusted p-value (log10)
Fold change gene expression (log2)
B
p53 target genes
S3I-201
NES = 2.96
FDR q = 0.0
S3I-201
DMSO
shSTAT3
NES = 1.59
FDR q = 0.0
shSTAT3
shSCR
Enrichment score
C
DMSO
S3I-201
Nap
(kDa)
p53
Tubulin
50
50
Relative p53 expression
DMSO
S3I
Nap
D
shSCR
sh1
(kDa)
STAT3
p53
Tubulin
80
50
50
Relative p53 expression
shSCR
sh1
shSTAT3
E
Con gRNA
gSTAT3
g1
g2
(kDa)
STAT3
p53
GAPDH
80
50
30
Relative p53 expression
Con gRNA
g1
g2
gSTAT3
F
Relative gene CDKN1A expression
DMSO
S3I
Nap
G
Relative gene CDKN1A expression
shSCR
sh1
shSTAT3
H
Relative gene CDKN1A expression
Con gRNA
g1
g2
gSTAT3

Figure 2

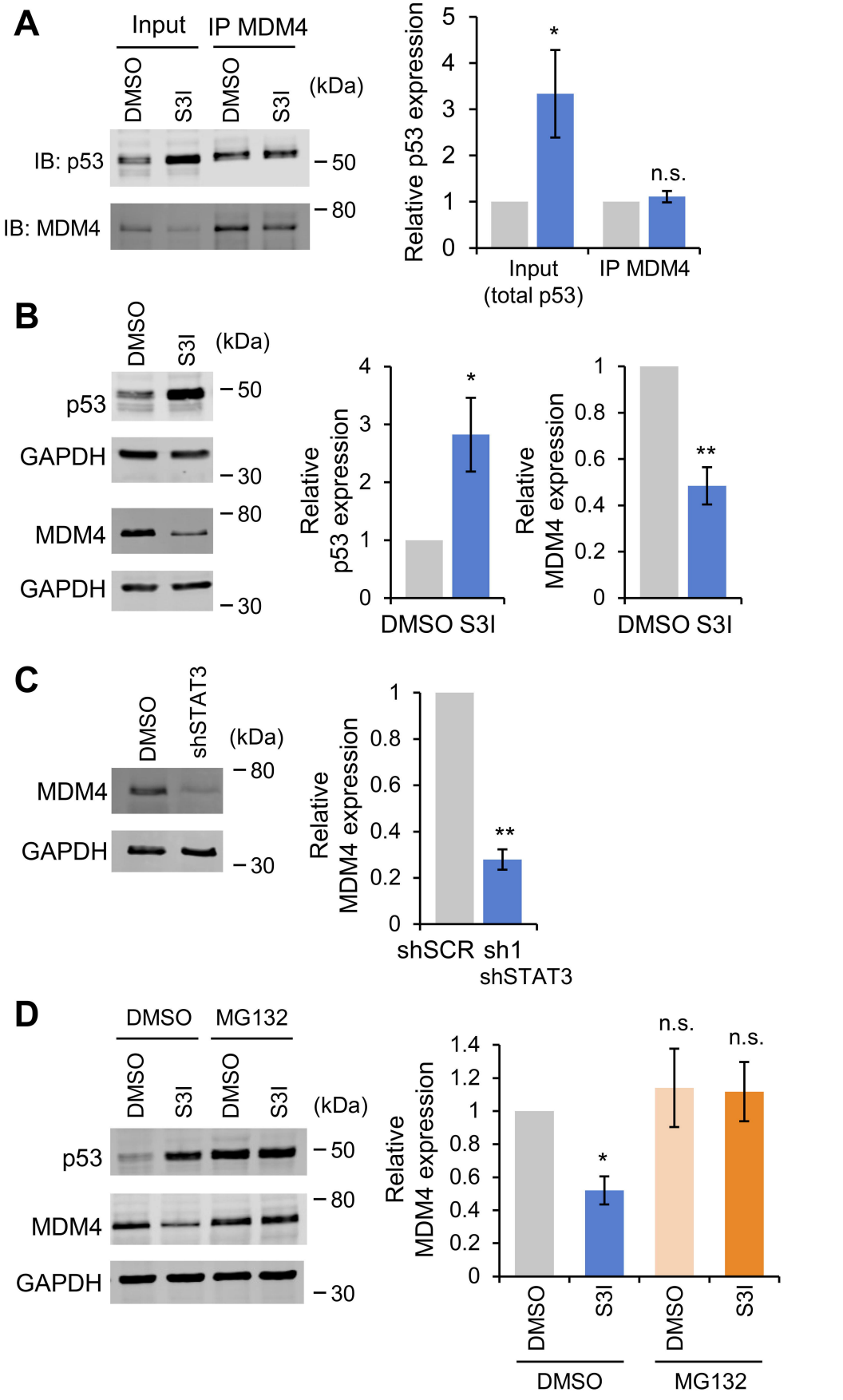
A
Input
IP MDM4
DMSO
S3I
DMSO
S3I
(kDa)
IB: p53
IB: MDM4
50
80
Relative p53 expression
5
4
3
2
1
0
*
n.s.
Input
(total p53)
IP MDM4
B
DMSO
S3I
(kDa)
p53
GAPDH
MDM4
GAPDH
50
30
80
30
Relative
p53 expression
4
3
2
1
0
*
DMSO S3I
Relative
MDM4 expression
1
0.8
0.6
0.4
0.2
0
**
DMSO S3I
C
DMSO
shSTAT3
(kDa)
MDM4
GAPDH
80
30
Relative
MDM4 expression
1
0.8
0.6
0.4
0.2
0
**
shSCR sh1
shSTAT3
D
DMSO
MG132
DMSO
S3I
DMSO
S3I
(kDa)
p53
MDM4
GAPDH
50
80
30
Relative
MDM4 expression
1.4
1.2
1
0.8
0.6
0.4
0.2
0
*
n.s.
n.s.
DMSO
S3I
DMSO
S3I
DMSO
MG132

Figure 3

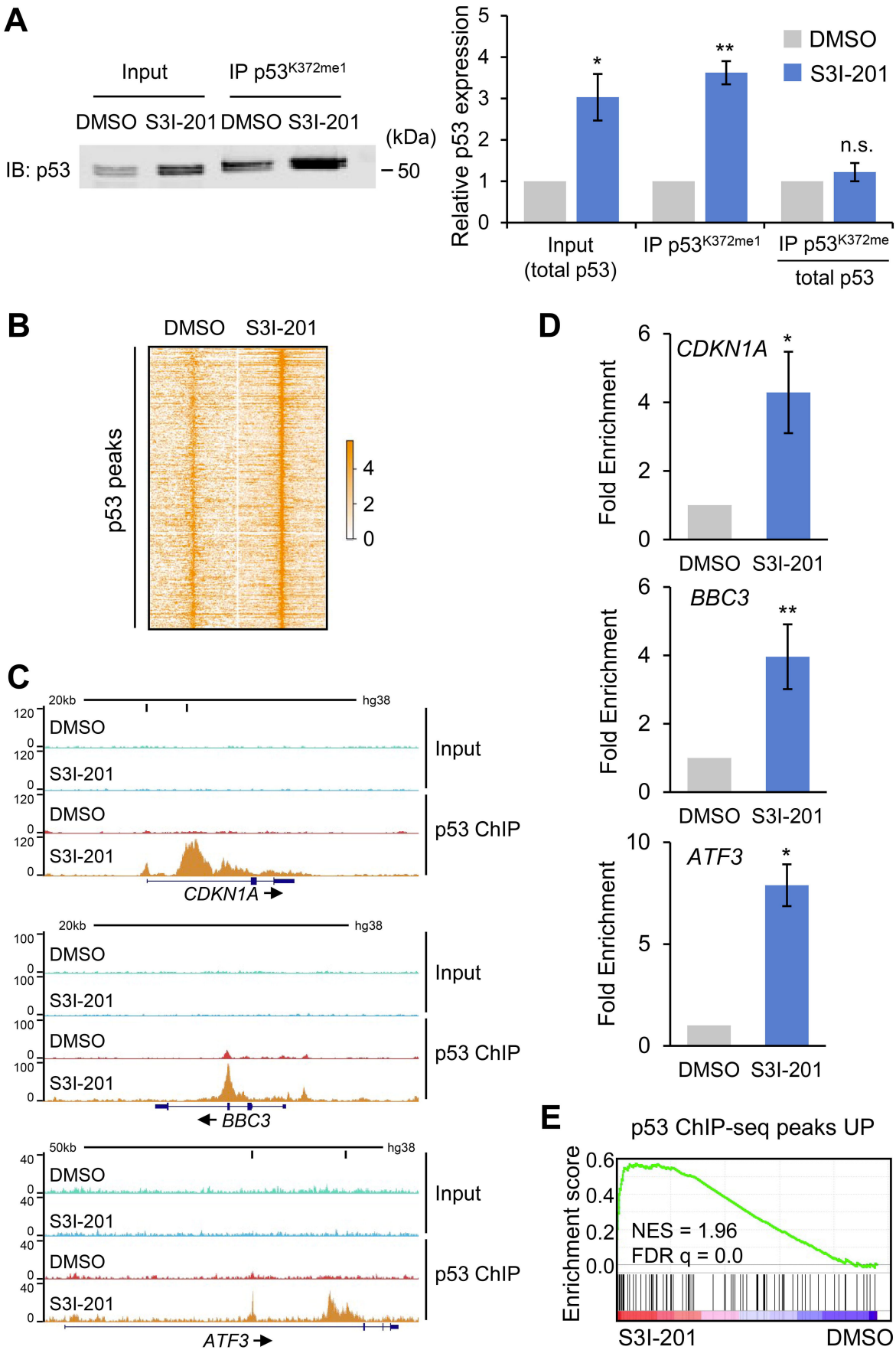
A
Input
IP p53K372me1
DMSO S3I-201 DMSO S3I-201
(kDa)
IB: p53
50
Relative p53 expression
DMSO
S3I-201
n.s.
Input (total p53)
IP p53K372me1
IP p53K372me total p53
B
DMSO S3I-201
p53 peaks
C
20kb
hg38
DMSO
S3I-201
Input
p53 ChIP
CDKN1A
BBC3
50kb
ATF3
D
CDKN1A
BBC3
ATF3
Fold Enrichment
E
p53 ChIP-seq peaks UP
Enrichment score
NES = 1.96
FDR q = 0.0
S3I-201
DMSO

Figure 4

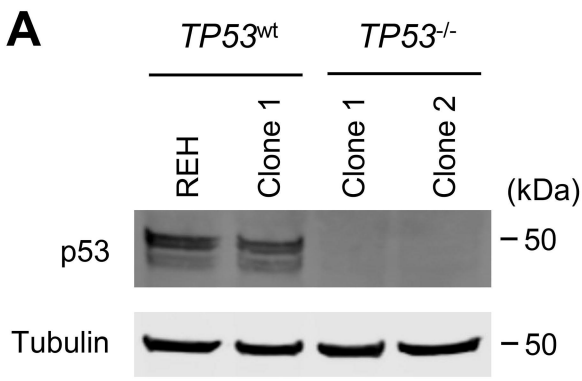
A
TP53wt
TP53-/-
REH
Clone 1
Clone 1
Clone 2
(kDa)
p53
50
Tubulin
50

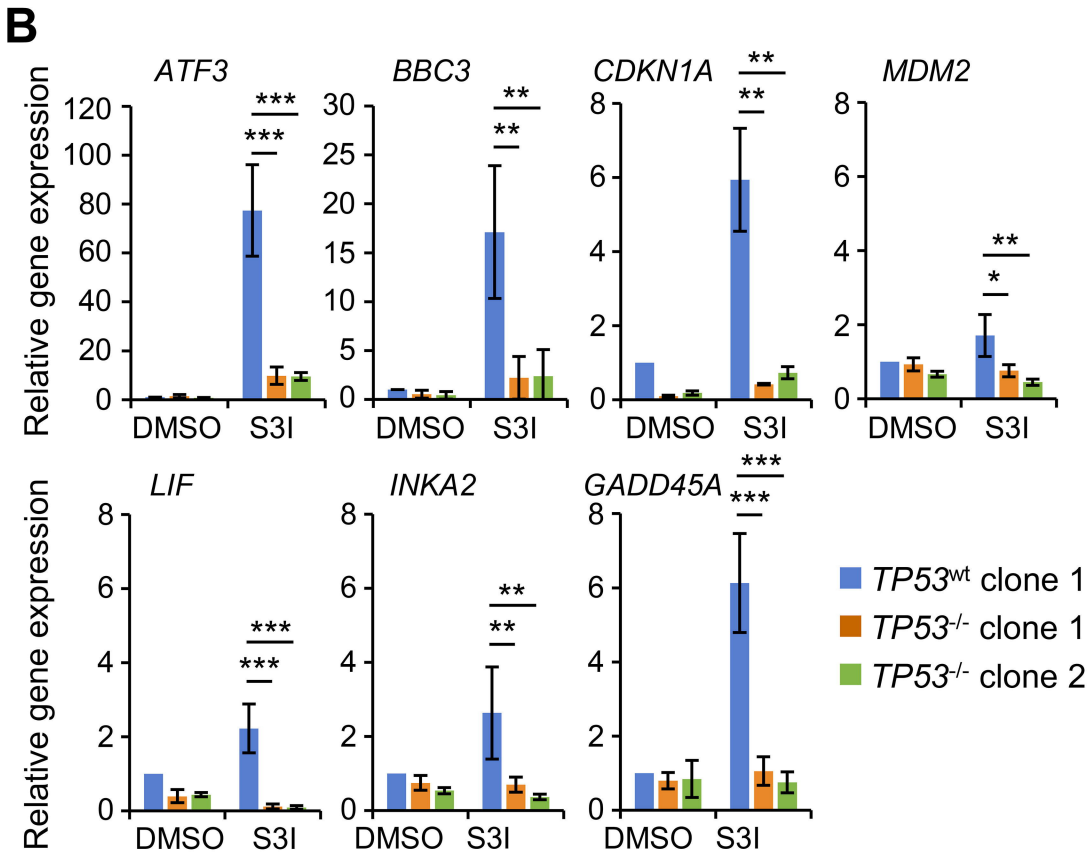
B
ATF3
BBC3
CDKN1A
MDM2
LIF
INKA2
GADD45A
Relative gene expression
DMSO
S3I
TP53wt clone 1
TP53-/- clone 1
TP53-/- clone 2

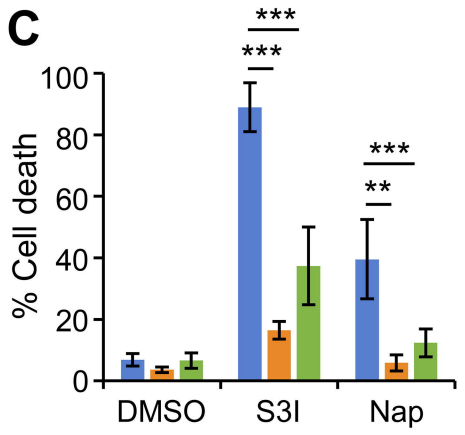
C
% Cell death
DMSO
S3I
Nap

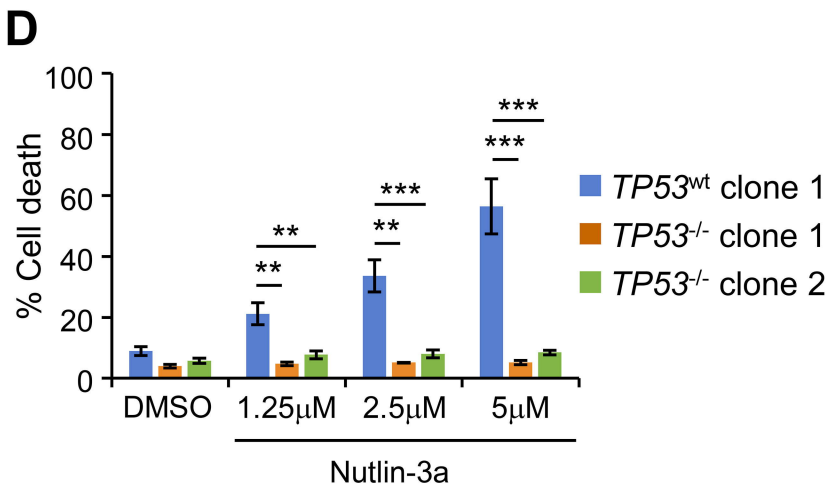
D
% Cell death
DMSO
1.25μM
2.5μM
5μM
Nutlin-3a
TP53wt clone 1
TP53-/- clone 1
TP53-/- clone 2

Figure 5

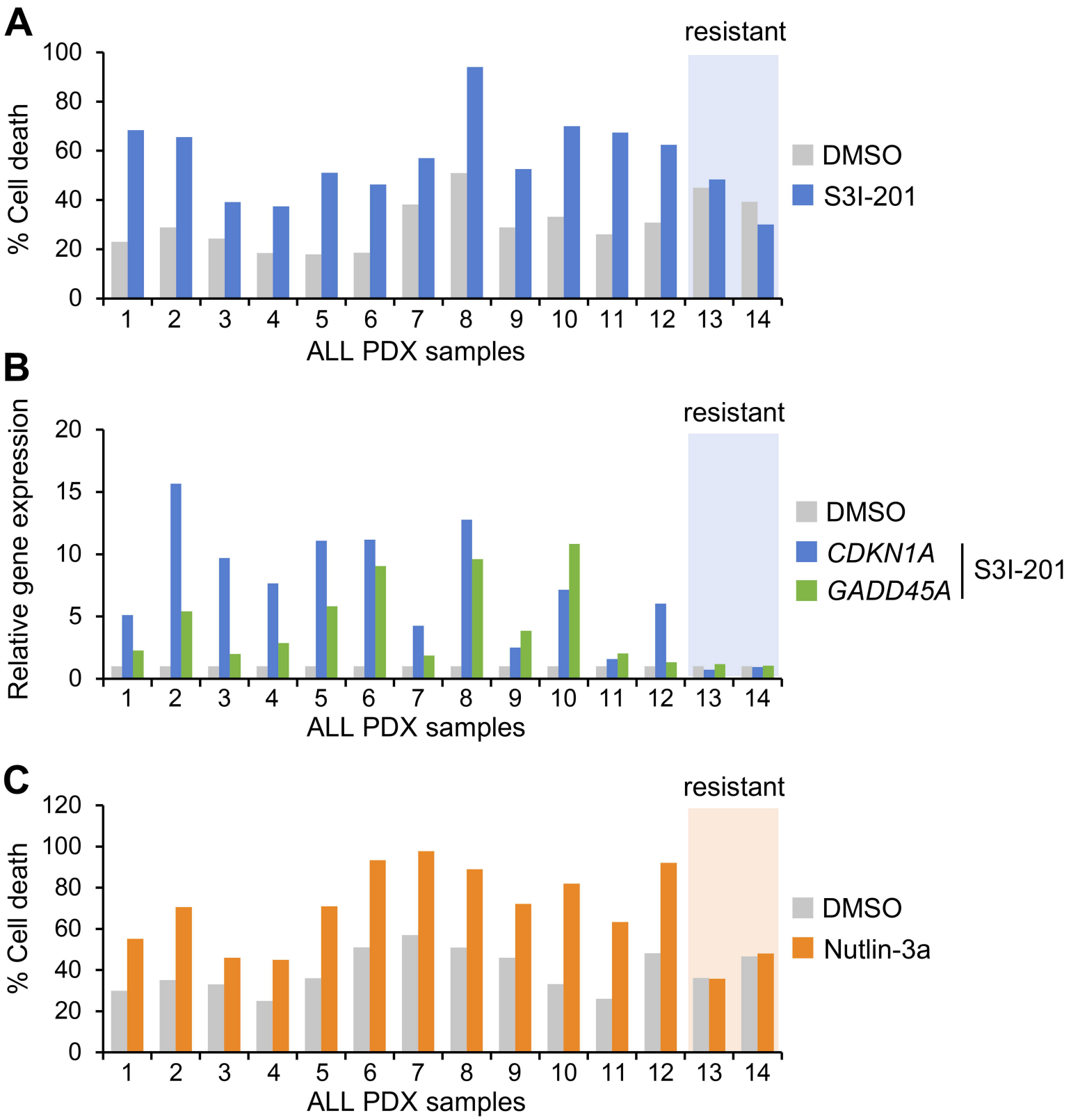
A
resistant
100
80
60
40
20
0
% Cell death
1 2 3 4 5 6 7 8 9 10 11 12 13 14
ALL PDX samples
DMSO
S3I-201
B
resistant
20
15
10
5
0
Relative gene expression
1 2 3 4 5 6 7 8 9 10 11 12 13 14
ALL PDX samples
DMSO
CDKN1A
GADD45A
S3I-201
C
resistant
120
100
80
60
40
20
0
% Cell death
1 2 3 4 5 6 7 8 9 10 11 12 13 14
ALL PDX samples
DMSO
Nutlin-3a

Figure 6

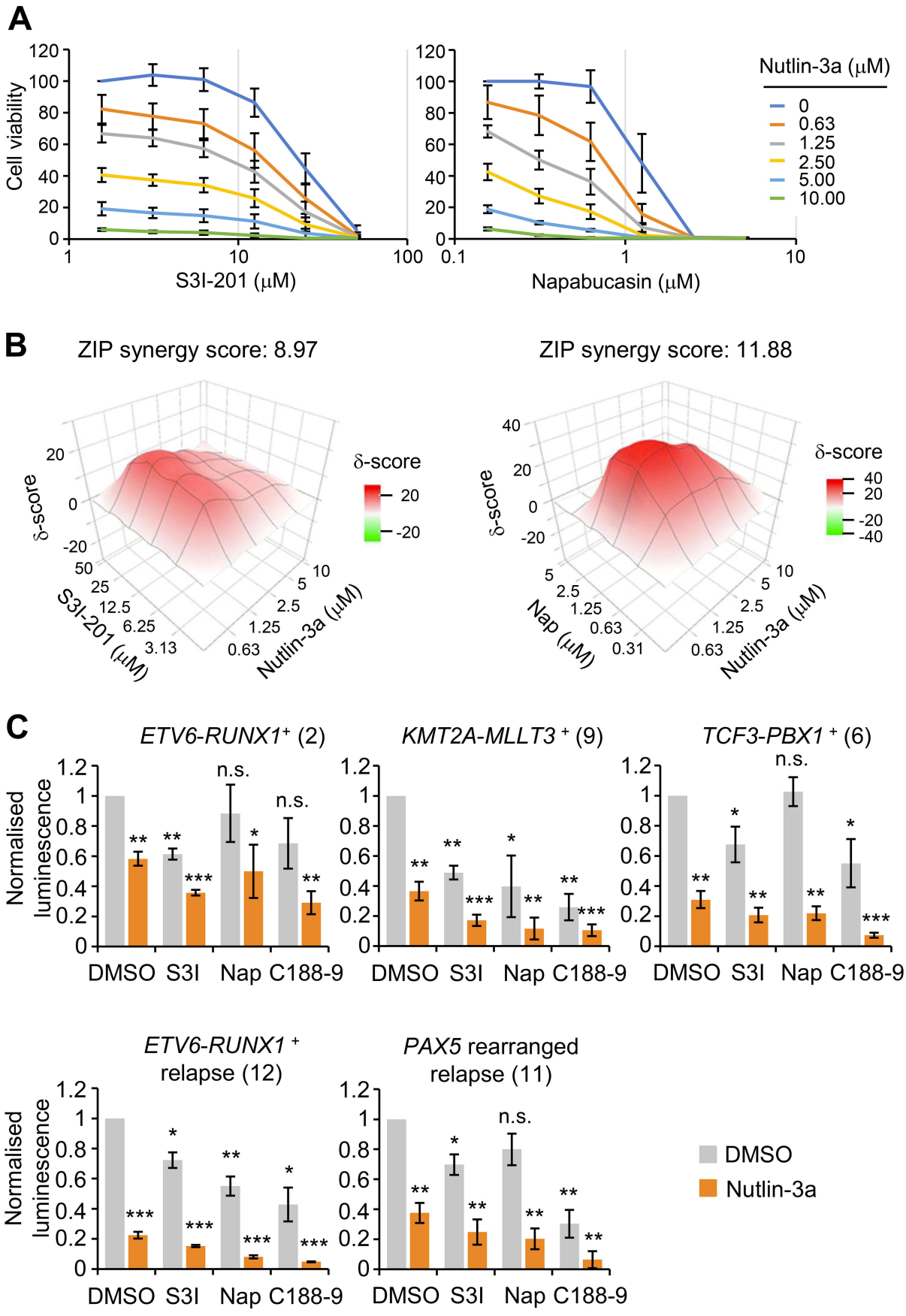
A
Cell viability
S3I-201 (μM)
Napabucasin (μM)
Nutlin-3a (μM)
0
0.63
1.25
2.50
5.00
10.00
B
ZIP synergy score: 8.97
ZIP synergy score: 11.88
δ-score
S3I-201 (μM)
Nutlin-3a (μM)
Nap (μM)
C
ETV6-RUNX1+ (2)
KMT2A-MLLT3 + (9)
TCF3-PBX1 + (6)
ETV6-RUNX1 + relapse (12)
PAX5 rearranged relapse (11)
Normalised luminescence
n.s.
DMSO
S3I
Nap
C188-9
DMSO
Nutlin-3a

Figure 7

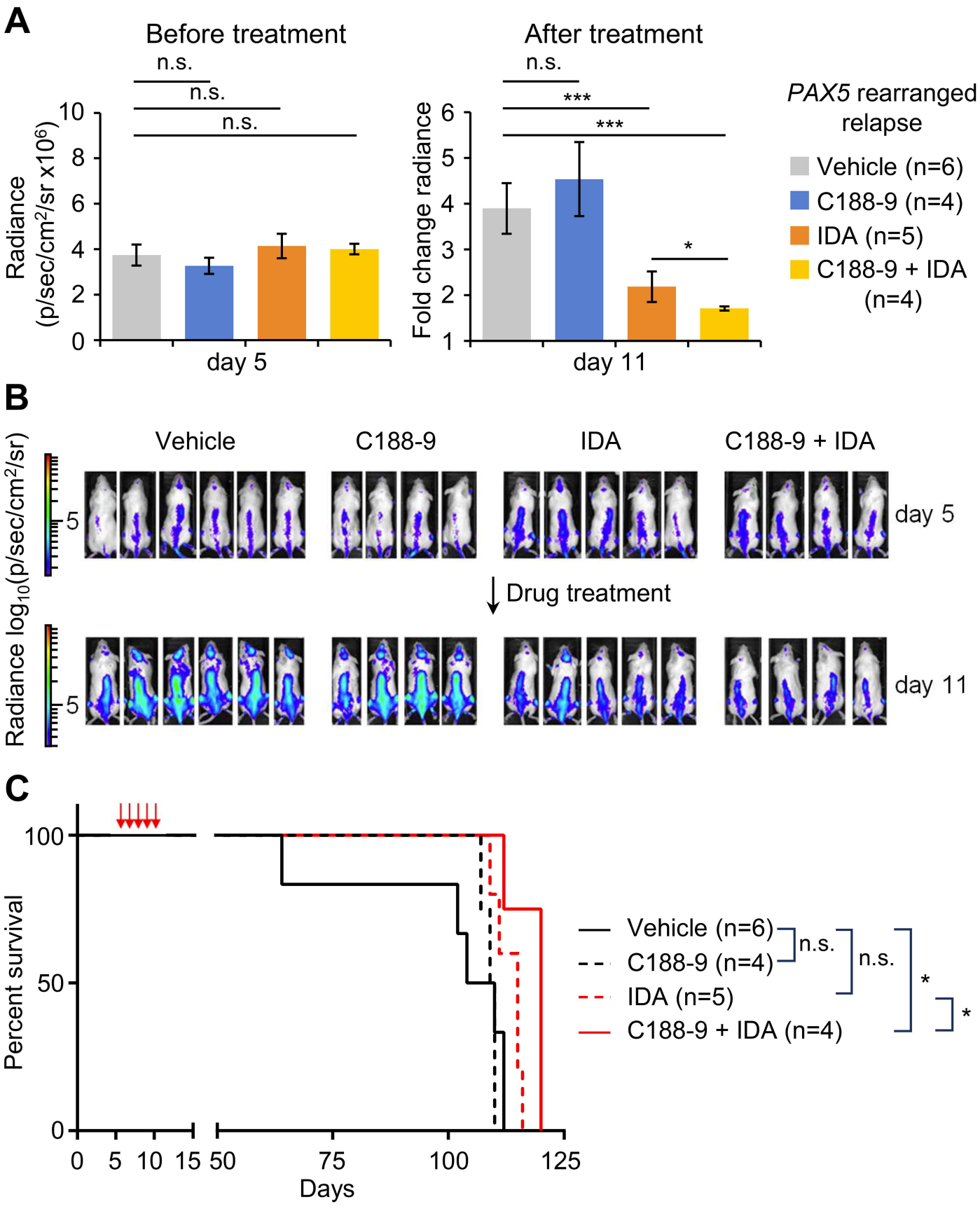
A
Before treatment
After treatment
n.s.
n.s.
n.s.
n.s.
***
***
*
Radiance (p/sec/cm²/sr x10⁶)
Fold change radiance
day 5
day 11
PAX5 rearranged relapse
Vehicle (n=6)
C188-9 (n=4)
IDA (n=5)
C188-9 + IDA (n=4)
B
Vehicle
C188-9
IDA
C188-9 + IDA
Radiance log10(p/sec/cm²/sr)
day 5
Drug treatment
day 11
C
Percent survival
Days
Vehicle (n=6)
C188-9 (n=4)
IDA (n=5)
C188-9 + IDA (n=4)
n.s.
n.s.
*
*

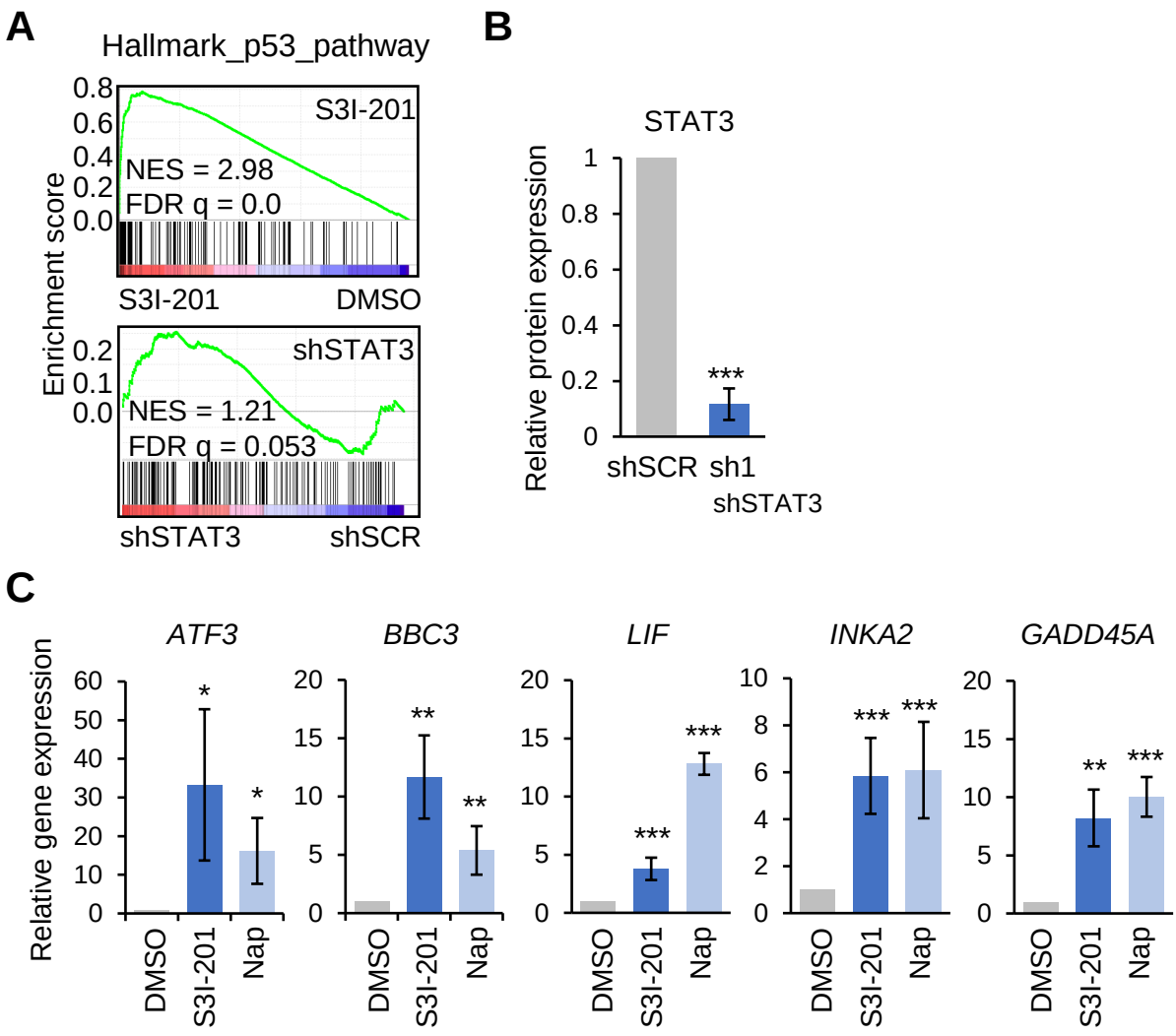

Supplementary Figure S1

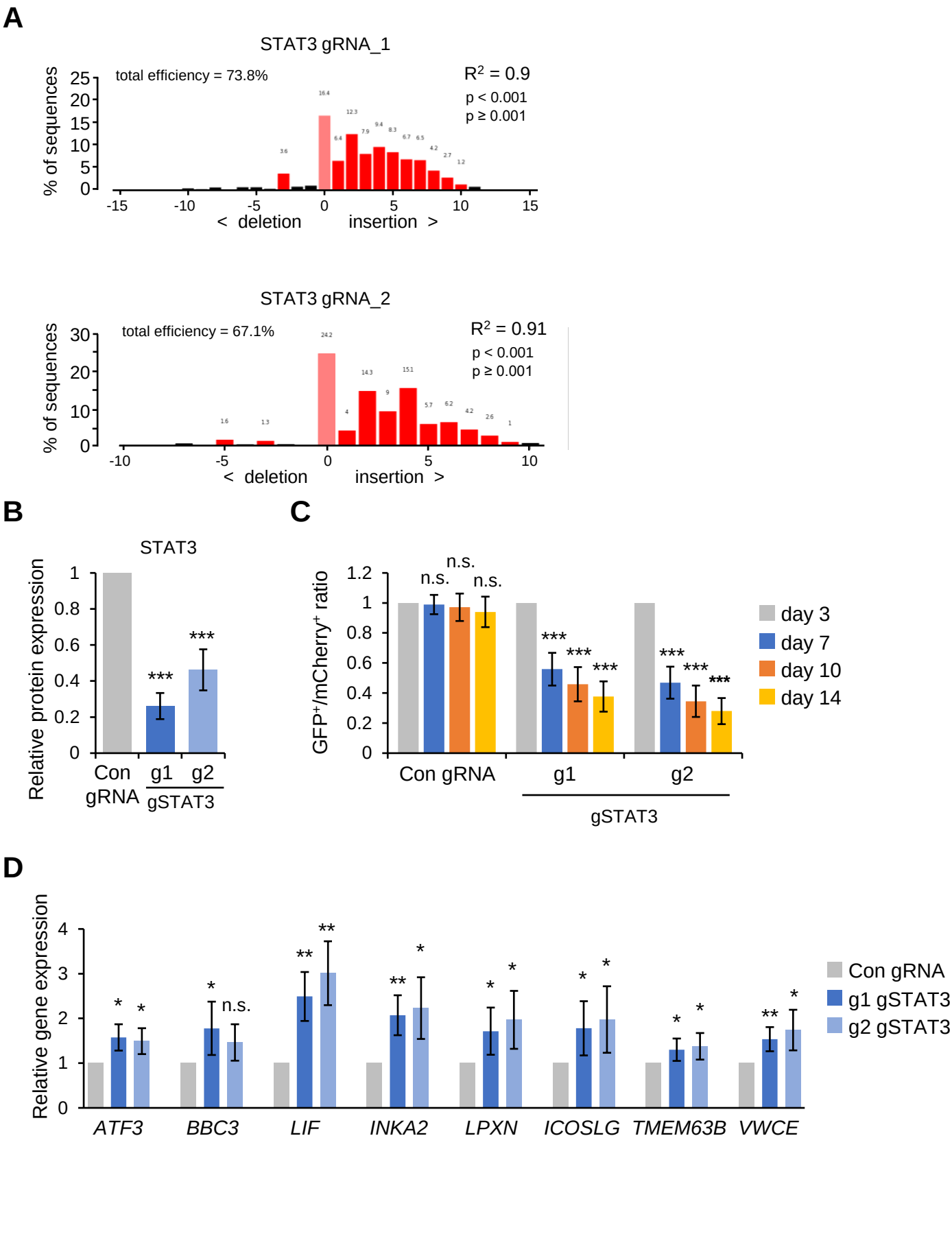

Supplementary Figure S2

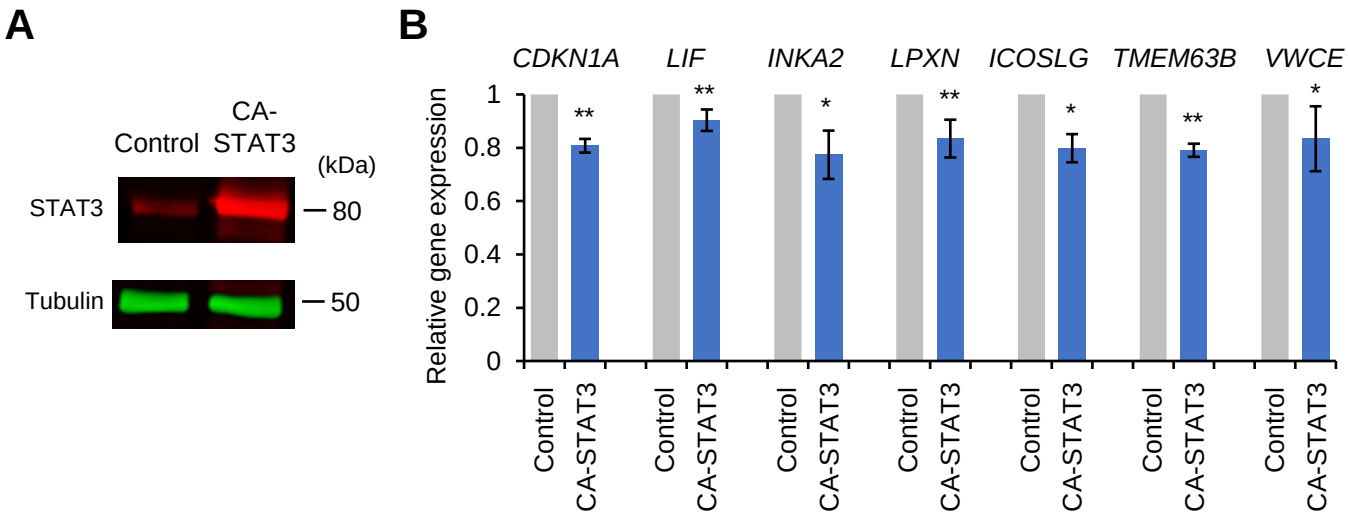

Supplementary Figure S3

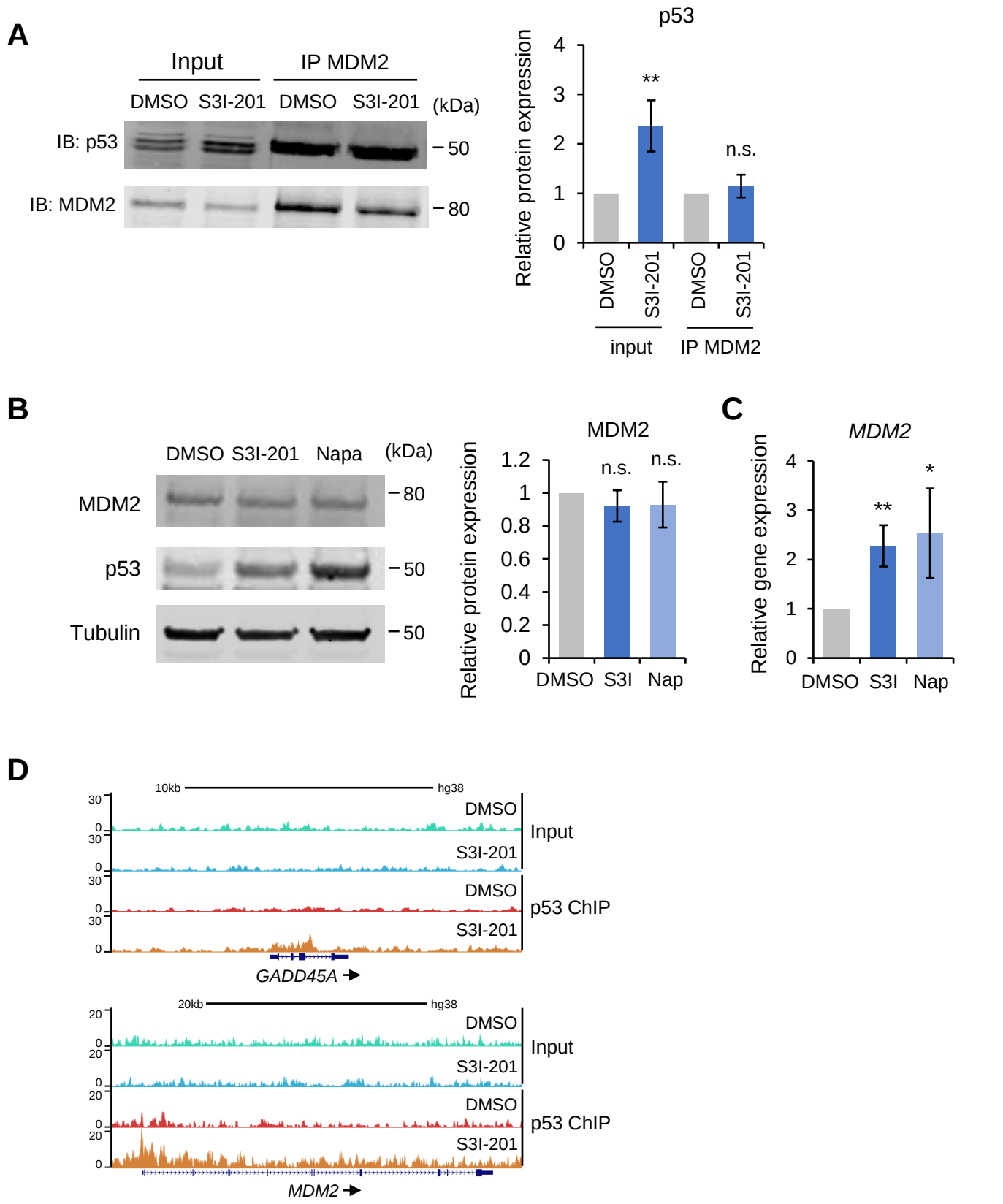

Supplementary Figure S4

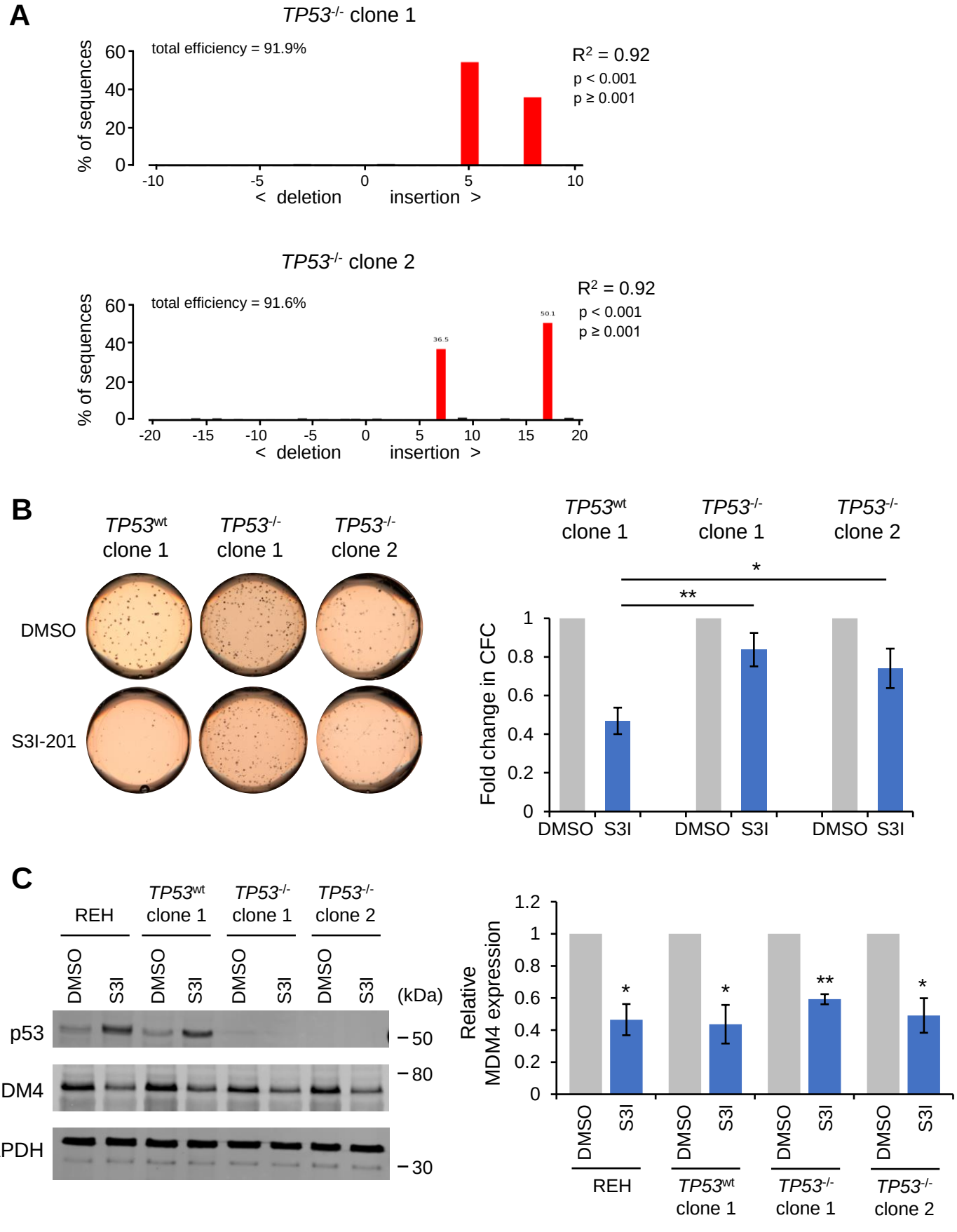

Supplementary Figure S5

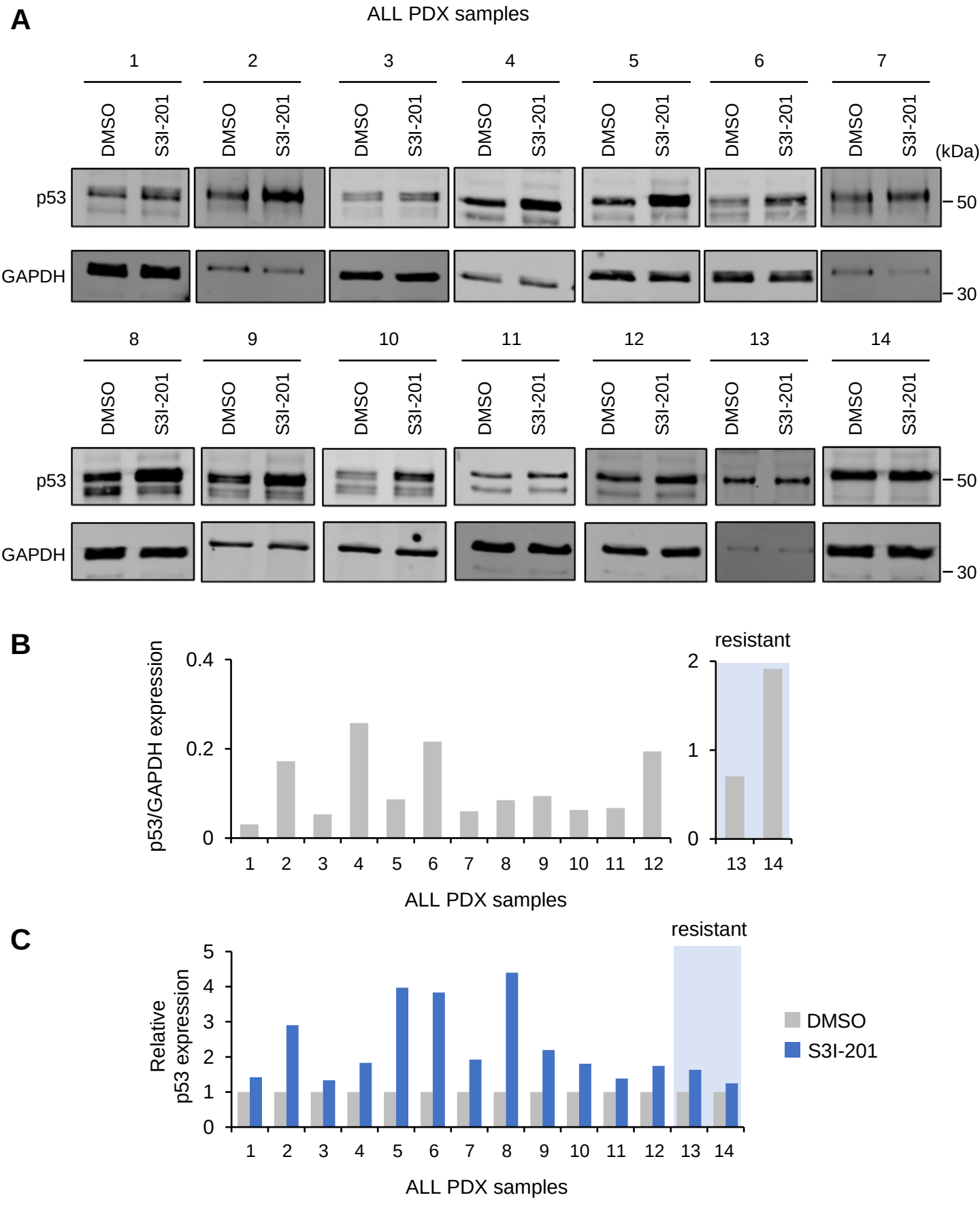

Supplementary Figure S6

A

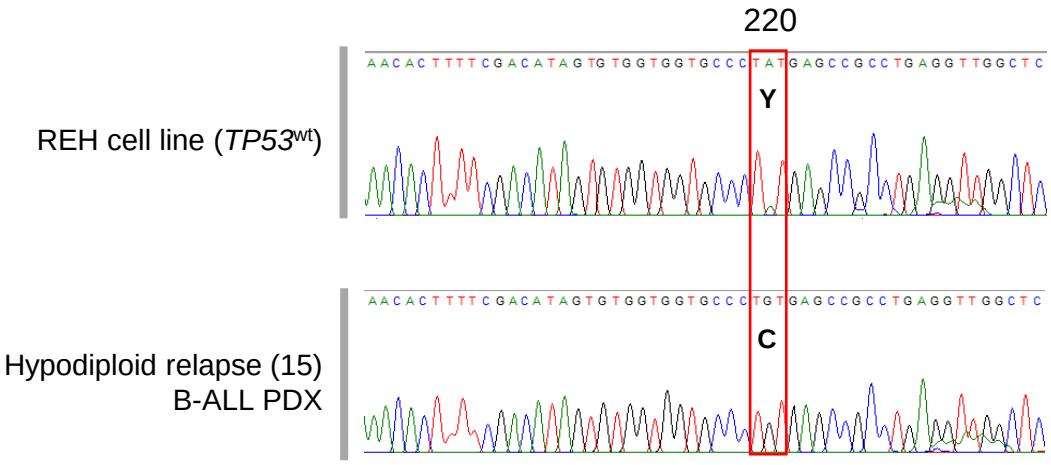

B

ETV6-RUNX1^{+} relapse (14) B-ALL PDX

Gene	Consequence	Location	HGVSc	HGVSp	VAF	TIER
TP53	**Missense variant**	chr17:7572938	c.1171G>C	p.Asp391His	0.416	TIER 3
TP53	**Splice acceptor variant**	chr17:7573009	c.1101-1G>A	NA	0.394	TIER 3
TP53	**Missense variant**	chr17:7577538	c.743G>A	p.Arg248Gln	0.470	TIER 2

Tier 2: potential clinical significance
Tier 3: variant of unknown clinical significance

Supplementary Figure S7

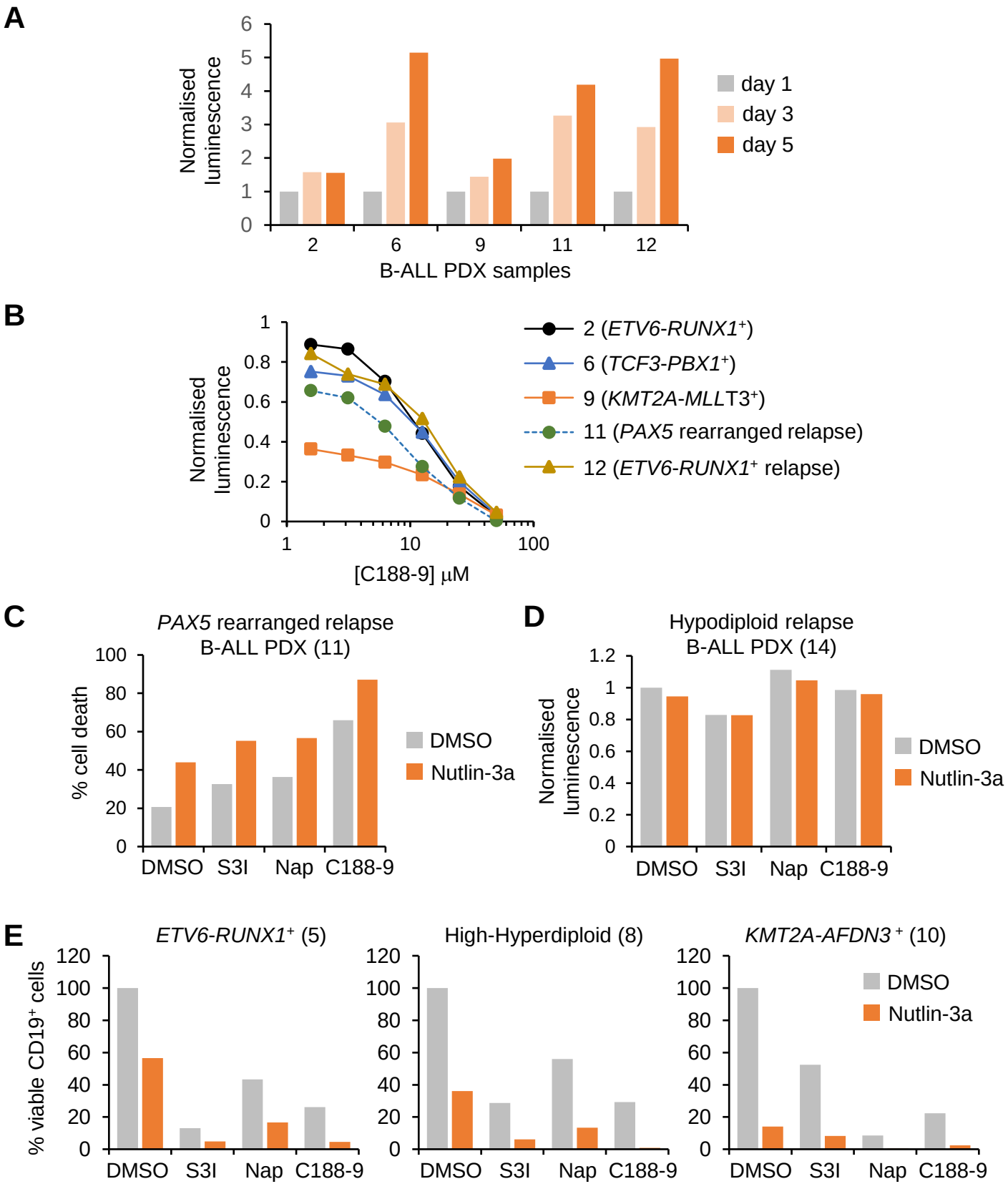

Supplementary Figure S8

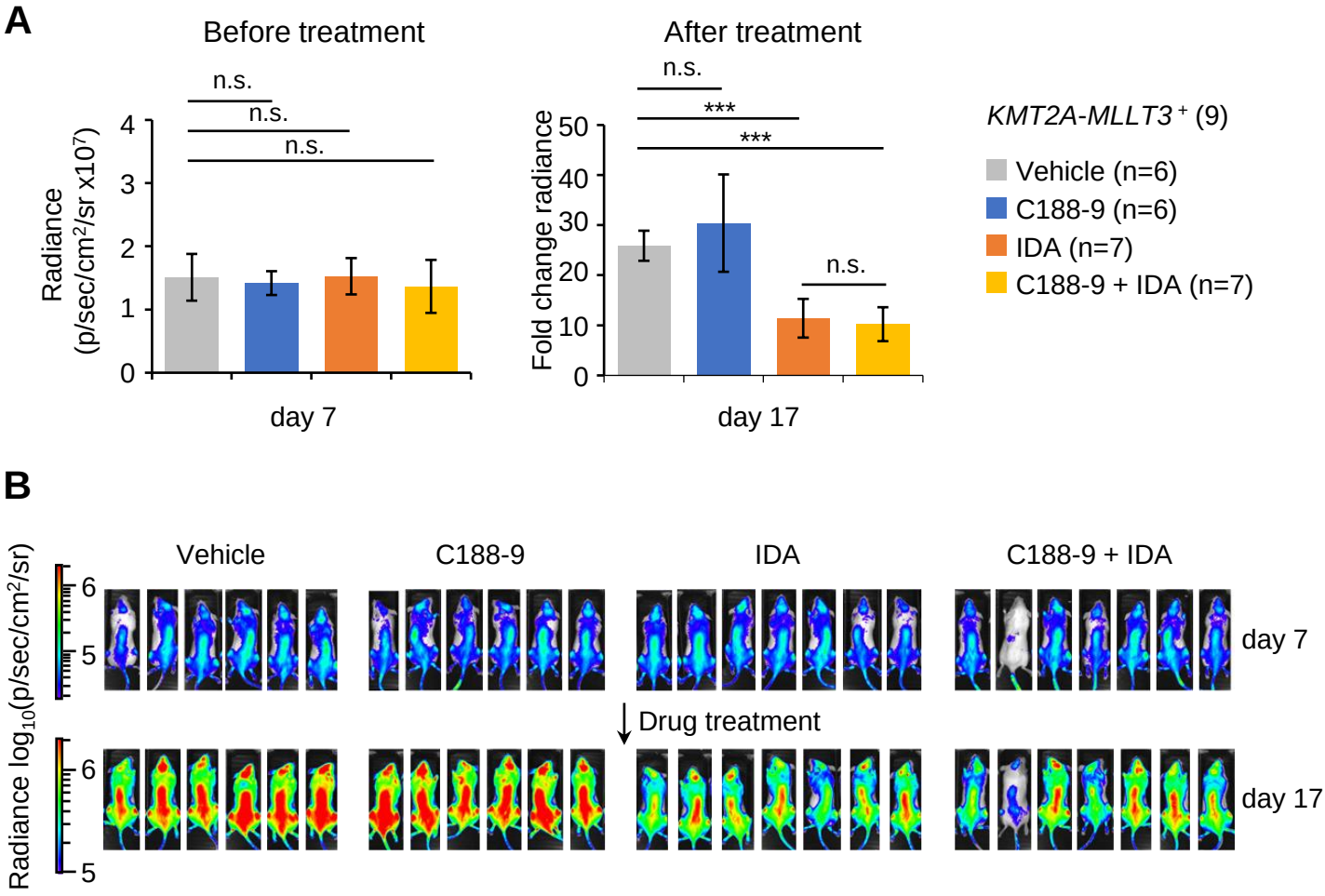

Supplementary Figure S9

Supplementary Figure Legends

Supplementary Figure S1. A GSEA demonstrating enrichment of the MSigDB hallmark p53 pathway gene set in S3I-201 (top panel) and shSTAT3 (lower panel) induced gene expression changes. **B** Western blot quantification of STAT3 protein expression in REH cells 5 days post transduction with control or shSTAT3 shRNA. Gene expression data are normalised to control shSCR transduced REH cells. Bars and error bars are means and SD of four independent experiments. ***$P < 0.001$, one sample *t* test. **C** qRT-PCR analysis of p53 target genes in REH cells following 6h treatment with either S3I-201 (50 μM) or Napabucasin (10 μM). Gene expression data are normalised to DMSO-treated cells. Bars and error bars are means and SD of n=5 independent experiments. *$P < 0.05$; **$P < 0.01$; ***$P < 0.001$, one sample *t* test.

Supplementary Figure S2. A TIDE (Tracking of Indels by Decomposition) analysis of CRISPR-Cas9 generated indels in REH cells transduced with Cas9 and gSTAT3 gRNA in a representative experiment**. B** Western blot quantification of STAT3 protein expression in REH cells 7 days post transduction with Cas9 and control or gSTAT3 gRNA. Bars and error bars are means and SD of n=5 independent experiments. Data are normalized to GAPDH loading control and to control gRNA transduced REH cells. ***$P < 0.001$, one sample *t*-test. **C** Data representing flow cytometric quantification of the relative proportions of GFP^+ or $mCherry^+$ REH cells at day 3, 7, 10 and 14 following transduction of REH cells with Cas9 and control or gSTAT3 gRNA. Cells were transduced with GFP-expressing GFP-CRISPR-Cas9-gRNA constructs or with an mCherry-expressing control empty vector (LeGO-iC2), mixed in a 1:1 ratio three days after transduction and resulting cultures subsequently monitored by flow cytometry. Bars and error bars are means and SD of n=4 independent experiments. ***$P < 0.001$;

n.s. not significant, one sample *t*-test. **D** qRT-PCR analysis of p53 target genes in REH cells 7 days post transduction with Cas9 and control or gSTAT3 gRNA. Gene expression data are normalised to control gRNA transduced REH cells. Bars and error bars are means and SD of n=4 independent experiments. *$P < 0.05$; **$P < 0.01$, one sample *t*-test.

Supplementary Figure S3. **A** Representative western blot analysis of STAT3 protein expression in REH 7 days following overexpression of constitutively activated STAT3 cDNA (*CASTAT3*). Tubulin was used as a loading control. **B** qRT-PCR analysis of p53 target genes in REH cells, 7 days following transduction with control empty vector or *CASTAT3*. Gene expression data are normalised to empty vector transduced REH cells. Bars and error bars are means and SD of n=3 independent experiments. *$P < 0.05$; **$P < 0.01$, one sample *t*-test.

Supplementary Figure S4. **A** Western blot analysis (left panel) and p53 protein expression quantification (right panel) of input and anti-MDM2 immunoprecipitates from REH cells, following 6 hours treatment with S3I-201 (50 μM). Blots were stained with anti-p53 (DO-1) or anti-MDM2 (OP-143). Data are normalized to DMSO-treated REH cells. Bars and error bars are means and SD of n=5 independent experiments. **$P < 0.01$; n.s. not significant, one sample *t*-test. **B** Western blot analysis (left panel) and quantification (right panel) of MDM2 and p53 protein expression in REH cells following 6h treatment with either S3I-201 (50 μM) or Napabucasin (10 μM). Tubulin was used as a loading control. Bars and error bars are means and SD of n=4 independent experiments. Data are normalized to Tubulin loading control and to DMSO-treated REH cells. n.s. not significant, one sample *t*-test. **C** qRT-PCR analysis

of *MDM2* gene expression level in REH cells following 6h treatment with either S3I-201 (50 μM) or Napabucasin (10 μM). Gene expression data are normalised to DMSO-treated cells. Bars and error bars are means and SD of n=5 independent experiments. *$P < 0.05$; **$P < 0.01$, one sample t-test. **D** Exemplar ChIP-Seq tracks for p53 peaks at target genes in DMSO and S3I-201 treated REH cells.

Supplementary Figure S5. **A** TIDE analysis of CRISPR-Cas9 generated indels in *TP53*$^{-/-}$ REH clones 1 and 2**. B** Representative example (left panel) and quantification (right panel) of *TP53*^{wt} or *TP53*$^{-/-}$ REH clone colony formation in methylcellulose cultures in the presence of DMSO or S3I-201 (50 μM). Fold change in colony forming capacity (CFC) relative to DMSO-treated cells is shown. Bars and error bars are means and SD of n=5 independent experiments. *$P < 0.05$, **$P < 0.01$, unpaired Student's *t* test between S3I-201-treated *TP53*^{wt} and *TP53*$^{-/-}$ clones. **C** Western blot analysis (left panel) and quantification (right panel) of MDM4 protein expression in REH cells, *TP53*^{wt} and *TP53*$^{-/-}$ clones following 6h treatment with S3I-201 (50 μM) or DMSO control. GAPDH was used as a loading control. Bars and error bars are means and SD of n=3 independent experiments. Data are normalized to GAPDH loading control and to DMSO-treated REH cells. *$P < 0.05$; **$P < 0.01$, one sample t-test.

Supplementary Figure S6. A Western blot analysis of p53 protein expression in B-ALL PDX samples 6h after exposure to S3I-201 (50 μM). **B** Quantification of p53 protein expression, relative to GAPDH loading control and **C** of p53 induction in S3I-201 treated cells relative to DMSO treated controls, in the PDX samples.

Supplementary Figure S7. A Sanger sequencing of a PCR amplified region of the *TP53* gene from the B-ALL REH cell line (upper panel) and Hypodiploid relapse (15) B-ALL PDX sample (lower panel). The TAT>TGT (Y220C) mutation was confirmed in this B-ALL PDX sample. **B** *TP53* somatic variants, identified via targeted capture panel sequencing, in the *RUNX1-ETV6*$^{+}$ relapse (14) B-ALL PDX sample. HGVSc (Human Genome Variation Society, coding); HGVSp (Human Genome Variation Society, protein); VAF (Variant Allele Frequency).

Supplementary Figure S8. A Luminescence of luciferase-expressing B-ALL PDX samples on days 1, 3 and 5 after plating onto human MSC. Data are normalised to luminescence values measured on day 1 of the co-cultures. B-ALL PDX samples: *ETV6-RUNX1*$^{+}$ (2), *TCF3-PBX1*$^{+}$ (6), *KMT2A-MLLT3*$^{+}$ (9), *PAX5* rearranged relapse (11), *ETV6-RUNX1*$^{+}$ relapse (12). **B** Luminescence of luciferase-expressing B-ALL PDX samples, grown in co-culture with human MSC, 5 days after exposure to the indicated concentrations of the STST3 inhibitor C188-9. Data are normalised to DMSO-treated cells. **C** Induction of apoptosis (% Annexin V^{+} cells) in the *PAX5* rearranged relapse (11) B-ALL PDX sample, grown in co-culture with human MSC, 72 hours after exposure to Nutlin-3a (5 μM) alone or in combination with STAT3 inhibitors S3I-201 (50 μM), Napabucasin (1.5 μM) and C188-9 (10 μM). Data are normalised to DMSO-treated cells. **D** Luminescence of luciferase-expressing Hypodiploid relapse (14) B-ALL PDX sample, grown in co-culture with human MSC, 5 days after exposure to Nutlin-3a (5μM) alone or in combination with STAT3 inhibitors S3I-201 (50 μM), Napabucasin (1.5 μM) and C188-9 (10 μM). Data are normalised to DMSO-treated cells. **E** Viability of untransduced B-ALL PDX samples, grown in co-culture with human MSC, 5 days after exposure to MDM2 inhibitor Nutlin-3a (5 μM) alone or in

combination with STAT3 inhibitors S3I-201 (50 μM), Napabucasin (1.5 μM) and C188-9 (10 μM), as determined by flow cytometry. Corresponding B-ALL PDX sample number from Figure 5 is indicated in brackets. Each bar represents the number of viable human $CD19^+$ ALL cells as a percentage of DMSO treated control cultures. The mean percentage of viable $CD19^+$ cells in DMSO treated triplicate control cultures at day 5 was 75.3% (PDX 5), 88.2% (PDX 8) and 85.9% (PDX 10).

Supplementary Figure S9. A Bioluminescence signal (radiance = photons/s/cm2/steradian) in NSG recipient mice 7 days after injection of the luciferase-expressing *KMT2A-MLLT3*$^+$ B-ALL PDX sample and before drug treatment (left panel), and fold change in bioluminescence signal 17 days after injection, following 7 daily treatments with vehicle or the indicated drug combinations (right panel). Bars and error bars are means and SD of values form each treatment group, the number of mice in each group indicated in brackets. ***$P < 0.001$; n.s. not significant, unpaired Student's *t* test between indicated groups. **B** Bioluminescence imaging of NSG recipient mice before (day 7) and after (day 17) drug treatment. Bars for luminescence signal represent photons/s/cm2/steradian.

Supplementary Table 1. Patient sample characteristics.

PDX sample	Classification	Sex	Age (yrs)	Cytogenetics
4	*ETV6-RUNX1*$^{+}$	F	1.92	ETV6-RUNX1 rearrangement detected in 60% of interphase nuclei.
5	*ETV6-RUNX1*$^{+}$	M	3.37	ETV6-RUNX1 fusion detected, showing clonal evolution involving gain of RUNX1 signal, by interphase FISH analysis.
6	*TCF3-PBX1*$^{+}$	F	10.95	Abnormal karyotype with a der(19)t(1;19) unbalanced translocation by G-banded analysis. Unbalanced TCF3-PBX1 rearrangement in 52% of nuclei and mono-allelic loss of CDKN2A in 5.5% nuclei by interphase FISH analysis.
7	Hyperdyploid	M	2.36	Gain of DXZ1, D9Z3, ABL1, RUNX1 and relative loss of one CDKN2A signal by FISH. Gain of chromosomes X, 9 and 21 by G-banded analysis.
8	High-Hyperdiploid	F	2.48	Abnormal high-hyperdiploid karyotype with gain of chromosomes X, 3, 5, 8, 10, 11, 12, 14, 17, 18, 21 and 22. Favourable prognosis.
9	*KMT2A-MLLT3*$^{+}$	F	2.52	KMT2A rearrangement with concomitant deletion of the 3'KMT2A region. t(9;11)(p22;q23).
10	*KMT2A-AFDN*$^{+}$	M	0.28	A t(6;11)(q27;q23) translocation identified in all metaphase spreads. FISH analysis confirmed a KMT2A rearrangement in 56% of nuclei.
11	*PAX5* rearranged (relapse)	M	5.10	PAX5 rearrangement in 92% cells by interphase FISH analysis. Consistent with CNS relapse of ALL.
12	*ETV6-RUNX1*$^{+}$ (relapse)	M	7.91	ETV6-RUNX1 rearrangement and bi-allelic deletion of CDKN2A detected in 69% and 72.5% nuclei, respectively. Additional copy of chromosome 21
13	*ETV6-RUNX1*$^{+}$ (relapse)	M	4.62	An ETV6-RUNX1 rearrangement detected in 76% nuclei examined by interphase FISH analysis.
14	Hypodiploid (relapse)	M	11.8	Hypodiploid with a doubled-up clone in a sub-population showing additional structural abnormalities, indicative of clonal evolution. FISH analysis showed loss of ETV6(73%), relative loss of centromere 17 (54%), and gain of signals for 11 and 17 centromeres (27%).

*PDX samples *ETV6-RUNX1* (1-3): patient samples characteristics previously reported in Mangolini et al (2013)

Supplementary Methods

Cell culture

Human B-ALL cell line REH was purchased from the ATCC. Cell lines were authenticated by short tandem repeat profiling using the PowerPlex 16 system (Promega, Southampton, UK) and mycoplasma negative status confirmed using the MycoAlert Mycoplasma Detection Kit (Lonza, Verviers, Belgium). Primary human MSC cells were obtained as described previously[1]. REH cells were cultured in Roswell Park Memorial Institute (RPMI), supplemented with 10% Foetal Bovine Serum (FBS), 100 U/ml Penicillin/100 µg/ml Streptomycin (Merck Life Science, Dorset, UK) and 2 mM L-glutamine (Merck Life Science). The HEK293FT packaging cell line was purchased from Thermofisher Scientific (Hemel Hempstead, UK) and cultured in Dublecco's Modified Medium (DMEM), supplemented with 10% FBS, 100 U/ml Penicillin/100 µg/ml Streptomycin and 2 mM L- glutamine. Primary human MSC cells were cultured in DMEM low glucose, supplemented with 20% FBS, 100 U/ml Penicillin/100 µg/ml Streptomycin, 2 mM L- glutamine and 8ng/ml Human FGF-basic (FGF-2/bFGF) (aa 10-155) recombinant protein (Thermofisher Scientific).

RNA sequencing (RNA-seq) and Gene set enrichment analysis (GSEA)

Total cellular RNA was purified from control and S3I-201-treated cells or shSTAT3 shRNA-transduced cells from three independent experiments each and submitted to UCL Genomics for RNA-sequencing. GSEA (https://software.broadinstitute.org/gsea/) was used to examine enrichment of the p53 target gene set[3] in RNA-seq data. Total cellular RNA was extracted using the RNeasy Plus Mini Kit (Qiagen, Manchester, UK) according to manufacturer's instructions. 100 ng of RNA per sample were analysed using Bioanalyser 2100 (Agilent Technologies, Santa Clara, CA) to verify RNA

integrity prior to amplification. Samples were processed using the Illumina TruSeq RNA sample prep kit Version2 (p/n RS-122-2001) according to manufacturer's instructions (Illumina, Cambridge, UK). Briefly, mRNA was selected using paramagnetic dT beads and fragmented by metal hydrolysis to approximately 150 bp lengths. Random primed cDNA was then generated and adapters compatible with Illumina sequencing were ligated before being enriched by 12 cycles of PCR. Libraries were quantified, normalised, and pooled before sequencing on an Illumina NextSeq 500, generating approximately 20 million 43 bp read pairs per sample. Fastq was then demultiplexed and generated using Illumina bcl2fastq v2.19 before pre-processing (trimmomatic) to remove adapter read-through and poor-quality sequences. Pre-processed data were then aligned to the genome (UCSC hg38) with Bowtie 2 and deduplicated using Picard. Reads-per-transcript were counted by FeatureCounts, before differential expression analysis by SARTools, a DESeq2 wrapper. All tools were invoked through the Galaxy Project for NGS analysis.

Colony-forming assays

Colony-forming ability was assessed by plating REH cells in methylcellulose (HSC002, Bio-Techne). Colonies were stained with 1 mg/ml p-iodonitrotetrazolium after 10 days of culture.

Synergy Experiments

$5x10^4$ REH cells were treated for 72h with S3I-201 or Napabucasin in combination with Nutlin-3a at indicated concentrations. Cell viability was evaluated with the CellTiter 96® AQueous One Solution Cell Proliferation Assay (Promega). ZIP synergy score was calculated using SynergyFinder (version 2.0) online software.[2]

Lentiviral transduction of human cell lines

293FT packaging cells (Thermo Fisher Scientific) were transiently co-transfected with the lentiviral expression vectors, the pCMV-PAX2 construct and the pVSV-G envelope construct (kind gifts of Prof D. Trono, Lausanne, Switzerland). Human leukemia cells were transduced with lentiviral supernatant by spinoculation at 700g, 25°C for 45 minutes in the presence of 5 μg/ml polybrene. After 2 days, transduced cells were selected in 1 μg/ml puromycin for 3 days. Lentiviral MISSION pLKO.1 shRNA constructs targeting *STAT3* (sh1, Clone ID:NM_003150.2-458s1c1; sh2, Clone ID:NM_003150.2-361s1c1) and the scramble (SCR) non-silencing control (SHC002) were purchased from Merck Life Science. CRISPR-Cas9 mediated knockout of *TP53* or *STAT3* in REH cells was performed with gRNA targeting *TP53* (CCATTGTTC AATATCGTCCGGGG) and *STAT3* (g1_STAT3 gRNA TGGGTGGAGAAGGACATC AGCGG; g2_STAT3 gRNA ACCCTGAGGGAGCAGAGATGTGG). *TP53*$^{-/-}$ REH clones were obtained by isolating individual colonies from methylcellulose cultures of bulk transduced REH cells.

Flow cytometry

Apoptosis was measured using the Annexin V Apoptosis Detection Kit (Thermo Fisher Scientific). Cells were acquired on a CytoFLEX (Beckman Coulter, High Wycombe, UK) and the data was analysed with CytExpert Software (Beckman Coulter).

Western blot and immunoprecipitation (IP) analysis

The following primary antibodies were used: anti-STAT3 (12640, Cell Signaling Technology, Leiden, The Netherlands), anti-TP53 (sc-126, Santa Cruz Biotechnology,

Texas, USA), anti-MDM2 (OP-143, Merck Life Science), anti-MDM4 (BL-3-2F2, Cambridge Bioscience, Cambridge, UK), anti-Tubulin (sc-53029, Santa Cruz Biotechnology), anti-GAPDH (sc-32233, Santa Cruz Biotechnology). IP analysis in REH cells was performed using the Pierce™ Classic Magnetic IP/Co-IP Kit (ThermoFisher Scientific) according to manufacturer's instructions. 2 μg of anti-$p53^{K372me1}$ (ab16033, Abcam, Cambridge, UK) or 2 μg of anti-MDM2 (sc-965, Santa Cruz Biotechnology) were used in each immunoprecipitation reaction. Protein samples were resolved on 10 % polyacrylamide gels (0.36 M bis-Tris, 8-10 % acrylamide/bis) in MOPS-SDS running buffer (50 mM Tris, 50 mM MOPS, 1 mM EDTA, 0.1 % SDS). Gels were transferred onto nitrocellulose (LI-COR Biosciences, Cambridge, UK) membranes. Proteins were detected using appropriate IRDye 800CW and IRDye 680RD labelled secondary antibodies (LI-COR Biosciences). Quantification was performed on fluorescent images using the Odyssey® CLx and Image Studio software (LI-COR Biosciences).

Chromatin immunoprecipitation (ChIP), ChIP-quantitative PCR (ChIP-qPCR) and sequencing (ChIP-seq)

$25x10^6$ REH cells were treated for 6h with either S3I-201 (50 μM) or DMSO and then were cross-linked with 2 mM DSG for 30 minutes at room temperature. After washing the samples 3 times with PBS, cells were fixed with 1% formaldehyde for 10 minutes at room temperature. The reaction was quenched by adding glycine to final concentration 0.125 M for 5 minutes at room temperature. Fixed cells were washed twice with cold PBS, and then sequentially in lysis buffer A (0.25% TritonX100, 10 mM EDTA, 0.5 mM EGTA, 20 mM HEPES [pH 7.6]) and lysis buffer B (150 mM NaCl, 10 mM EDTA, 0.5 mM EGTA, 20 mM HEPES [pH 7.6], incubating for 10 minutes in

rotation at 4°C each time. Cells were then resuspended in incubation buffer (0.15% SDS, 1% TritonX100, 150 mM NaCl, 10 mM EDTA, 0.5 mM EGTA, 20 mM HEPES [pH 7.6]) plus protease inhibitors (Roche, Merck) and incubated for 30 minutes on ice. Lysates were then sonicated for 20 cycles (30 sec on / 30 sec off) in the Bioruptor Pico water bath sonicator (Diagenode, Liege, BE). Cleared supernatant was stored at -80°C. 250 µl of sonicated chromatin were diluted in incubation buffer supplemented with 0.1% BSA and protease inhibitors and were incubated rotating at 4°C overnight, with protein A magnetic beads (Merck Life Science) and 2 µg of anti-TP53 (C15410083 ,Diagenode) antibody. Beads were washed for 10 minutes twice in low salt buffer (0.1% SDS, 0.1% DOC, 1% Triton X-100, 0.1 mM EDTA pH 8.0, 0.5 mM EGTA, 10 mM Tris-HCl [pH 8.0], 150 mM NaCl), and once in high salt buffer (0.1% SDS, 0.1% DOC, 1% Triton X-100, 0.1 mM EDTA pH 8.0, 0.5 mM EGTA, 10 mM Tris-HCl [pH 8.0], 500 mM NaCl), LiCl Buffer (250 mM LiCl, 0.5% DOC, 0.5% NP-40, 0.1 mM EDTA, 0.5 mM EGTA, 10 mM Tris-HCl [pH 8.0]) and in TE buffer (10 mM Tris-HCl [pH 8.0], 0.1 mM EDTA, 0.5 mM EGTA). DNA was eluted from the ChIP samples by 20 minutes incubation in rotation at RT with elution buffer (1% SDS, 100 mM $NaHCO_3$). Chromatin was reverse-crosslinked and subjected to RNase and proteinase K digestion and extracted by using the MinElute PCR purification kit (Qiagen). ChIP-qPCR experiments were performed on the purified DNA using SensiFAST™ SYBR® Hi-ROX Kit (Meridian Bioscience, TN, United States). Primers were designed with Primer3web (version 4.1.0) and were as follows: *CDKN1A* forward: CTCTGGCATAGAAGAGGCTGG; *CDKN1A* reverse: GGCTAAGGTTTACCTGGGGTC; *BBC3* forward: TACTGTGCGTTGAGGTCGT; *BBC3* reverse: CGGGGAGGAGGAACAGTG; *ATF3* forward: CACACACCTGGGACTCTCAC; *AFT3* reverse: TATCTGCACAAGTGGCTCCA;

Gene Desert 21 forward: GGGGGATCAGATGACAGTAAA; Gene Desert 21 reverse: AATGCCAGCATGGGAAATA. For ChIP-seq, libraries were prepared from 1ng of ChIP DNA using the NEBNext DNA Ultra II assay (New England Biolabs, Hitchin, UK) with bead-based size selection for 200 bp fragments and 12 cycles of amplification. Samples were then sequenced on an Illumina NextSeq 500, using a 43bp, paired end configuration. Fastq was then demultiplexed and generated using Illumina bcl2fastq v2.19 before pre-processing (trimmomatic) to remove adapter read-through and poor-quality sequences. Pre-processed data were aligned to the genome (UCSC hg38) with BWA14 and deduplicated. Peak calling was conducted using MACS1.3.3[4] at a *P*-value cut-off of 10^{-6}. Bigwig files were generated using bam2bw. Tags within a given region were counted and adjusted to represent the number of tags within a 1 kb region. Subsequently the percentage of these tags as a measure of the total number of sequenced tags of the sample was calculated and displayed as a heat map as before.[5,6]

In vivo transplantation

6-10 week old female NOD-SCID-$\gamma^{-/-}$ (NSG) mice were used as recipients for transplantation. Group sizes were chosen based on previous estimates of disease progression in transplanted mice and experiments in the literature performing similar studies. No samples or animals were excluded from analysis.

References

1. Pal D, Blair HJ, Elder A, et al. Long-term in vitro maintenance of clonal abundance and leukaemia-initiating potential in acute lymphoblastic leukaemia. Leukemia. 2016;30(8):1691-1700.

2. Ianevski A, Giri AK, Aittokallio T. SynergyFinder 2.0: visual analytics of multi-drug combination synergies. Nucleic Acids Res. 2020;48(W1):W488-W493.
3. Fischer M. Census and evaluation of p53 target genes. Oncogene. 2017;36(28):3943-3956.
4. Zhang Y, Liu T, Meyer CA, et al. Model-based analysis of ChIP-Seq (MACS). Genome Biol. 2008;9(9):R137.
5. Mandoli A, Singh AA, Prange KHM, et al. The Hematopoietic Transcription Factors RUNX1 and ERG Prevent AML1-ETO Oncogene Overexpression and Onset of the Apoptosis Program in t(8;21) AMLs. Cell Rep. 2016;17(8):2087-2100.
6. Prange KHM, Mandoli A, Kuznetsova T, et al. MLL-AF9 and MLL-AF4 oncofusion proteins bind a distinct enhancer repertoire and target the RUNX1 program in 11q23 acute myeloid leukemia. Oncogene. 2017;36(23):3346-3356.